THE ASTROPHYSICAL JOURNAL, 524:434–453, 1999 October 10

EXPLOSIVE HYDROGEN BURNING OF ^{27}Si, ^{31}S, ^{35}Ar, AND ^{39}Ca IN NOVAE AND X-RAY BURSTS

CHRISTIAN ILIADIS
University of North Carolina at Chapel Hill, and Triangle Universities Nuclear Laboratory, Durham, NC 27708-0308; iliadis@tunl.duke.edu
PIETER M. ENDT
R. J. Van de Graaff Laboratorium, Universiteit Utrecht, P.O. Box 80000, 3508 TA Utrecht, Netherlands
NIKOS PRANTZOS
Institut d'Astrophysique de Paris, 98bis Boulevard Arago, F-75014 Paris, France; prantzos@iap.fr
AND
WILLIAM J. THOMPSON
University of North Carolina at Chapel Hill, Chapel Hill, NC 27599-3255; wmjthompson@msn.com
Received 1998 April 24; accepted 1999 May 28

ABSTRACT

Stellar reaction rates for proton captures on the nuclei ^{27}Si, ^{31}S, ^{35}Ar, and ^{39}Ca are estimated from the most recent nuclear structure information available. Reliable mirror-state correspondences are found by using the isobaric multiplet mass equation. An improved method for calculating proton partial widths is applied. Systematic comparisons of excitation energies, spectroscopic factors, proton partial widths, and γ-ray partial widths for states of the same isospin multiplet are presented. Stellar reaction-rate uncertainties are deduced, and our reaction rates are compared to previous estimates. Reaction network calculations are performed to investigate implications of the new reaction rates for nucleosynthesis in novae and X-ray bursts. Our recommended reaction rates are varied within their assigned uncertainties, and we find only minor effects on the nuclear energy generation and the final abundances after the outbursts. Thus, contrary to previous claims, we find no compelling reason for measuring the proton capture reactions on ^{27}Si, ^{31}S, ^{35}Ar, and ^{39}Ca by using radioactive ion beams.

Subject headings: novae, cataclysmic variables — nuclear reactions, nucleosynthesis, abundances — X-rays: bursts

1. INTRODUCTION

Thermonuclear explosions induced by reactions involving hydrogen are expected to occur in classical novae (Politano et al. 1995; Gehrz et al. 1998) and in type I X-ray bursts (Lewin, van Paradijs, & Taam 1993; Taam, Woosley, & Lamb 1996). More exotic sites for this kind of nuclear burning include accreting black holes (Jin, Arnett, & Chakrabarti 1989; Arai & Hashimoto 1995), supermassive star explosions (Fuller, Woosley, & Weaver 1986), and Thorne-Zytkow objects (Biehle 1991; Cannon 1993). Early attempts to investigate the nucleosynthesis and energy production in explosive hydrogen-burning scenarios have considered predominantly proton-induced reactions on C, N and O seed nuclei. The resulting network of nuclear processes is known as the H(ot)CNO cycles and consists of a relatively small number of processes, such as (p, γ), (p, α) reactions and β^+-decays, involving nuclei in the mass $A < 20$ range. Most of these nuclear cross sections are important for understanding astrophysical events and therefore need to be measured in laboratory experiments. The measurements are straightforward if the target nuclei are stable. If the target nuclei are short lived, direct experimental measurements would require the use of accelerated radioactive ion beams. Several nuclear reactions important for hydrogen-burning scenarios were measured recently using this technique (Delbar et al. 1993; Coszach et al. 1995; Rehm et al. 1996). In fact, the study of astrophysically important nuclear reactions provides a strong motivation for the experimental program of existing and planned radioactive ion beam facilities.

It has been known for some time that under certain conditions explosive hydrogen burning is not restricted to proton-induced reactions on light target nuclei with masses $A < 20$. If the stellar temperature is sufficiently high or if a substantial number of heavy seed nuclei with masses $A \geq 20$ exist before the explosion, proton-capture reactions on a variety of heavier target nuclei are likely to occur. The resulting complicated network of nuclear processes is called the rp- (rapid proton capture) process (Wallace & Woosley 1981; Wiescher et al. 1986; Van Wormer et al. 1994). A quantitative understanding of the rp-process is more difficult compared to HCNO cycles, mainly because of the large number of possible nuclear reactions. For the same reason, the identification of nuclear reactions that could be of prime importance for radioactive ion beam experiments is no longer straightforward.

It is possible, however, to simplify this complex situation if nuclear reactions are systematically represented in terms of their reaction Q values. The result of a nuclear reaction network calculation, performed for explosive hydrogen-burning conditions, is shown in Figure 1 in order to illustrate this point. (Details regarding the calculations can be found in § 4.) Below mass $A = 20$, the abundance flow pattern reflects the operation of the HCNO cycles consisting of a restricted number of nuclear processes. Above mass $A = 20$, the rp-process forms an extended network of many nuclear reactions and decays. In Figure 1 we have indicated with the same color short-lived target nuclei that have similar Q values for proton-capture reactions. It can be seen that a periodic pattern emerges, which reflects the dependence of nuclear binding energies (or masses) on the pairing force. Consequently, the different nuclear target mass series can be discussed separately.

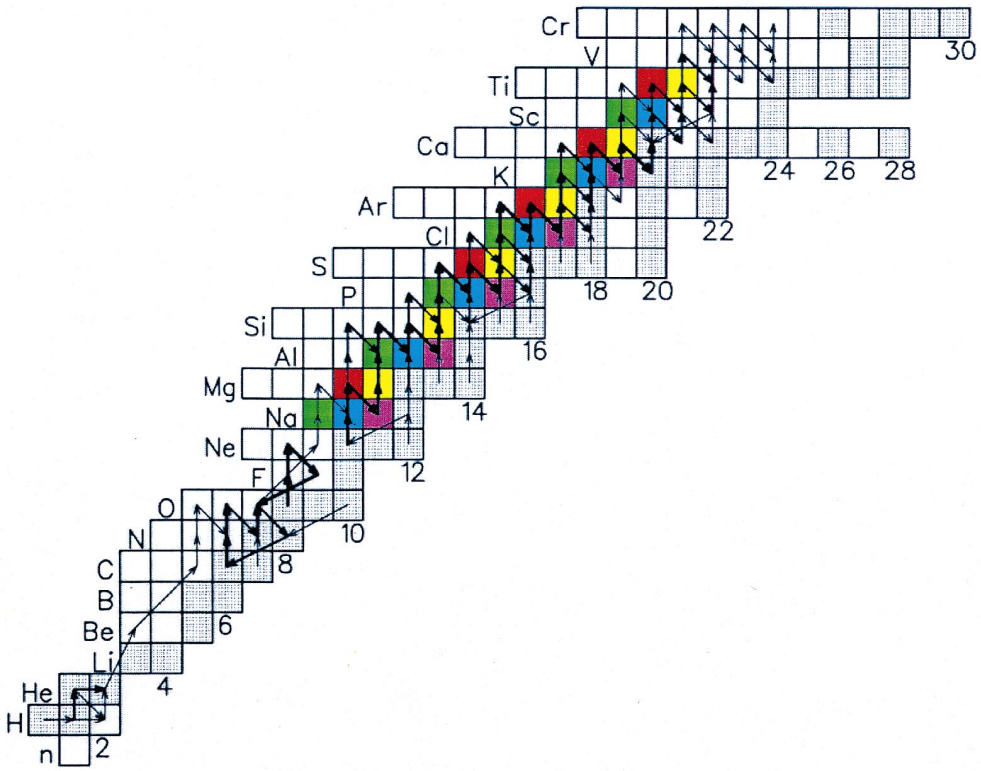

FIG. 1.—Nuclear abundance flows across the nuclidic chart, calculated for constant temperature and density conditions of $T_9 = 0.4$ and $\rho = 10^4$ g cm^{-3}, respectively, and a total time period of 10 s. For details regarding the network calculations, see § 4. Target nuclei with $Q_{p\gamma}$ values (Audi & Wapstra 1995) in the ranges of $\leq$0.5, 0.5–2.0, 2.5–3.5, 3.5–5.5 and 5.5–7.5 MeV are represented by the red, yellow, green, blue, and purple squares, respectively.

If a (p, γ) reaction has a high Q value (say, several MeV, for target nuclei represented by the green, blue, and purple squares in Fig. 1), the corresponding level density in the compound nucleus is most likely large enough that the statistical model of nuclear reactions can be applied to estimate stellar reaction rates (see, for example, Rauscher, Thielemann, & Kratz 1997). Therefore, a detailed knowledge of properties for specific nuclear levels is not necessary. On the other hand, if the Q value of a (p, γ) reaction is very low ($Q < 0.5$ MeV, for target nuclei represented by the red squares in Fig. 1), the inverse photodisintegration reaction becomes important at the elevated temperatures typical of explosive hydrogen burning. In this case, the nucleosynthesis depends mainly on the ratio of forward (proton capture) to backward (photodisintegration) reaction rates. According to the principle of time-reversal invariance, this ratio is determined by the (p, γ) reaction Q value and is independent of the particular reaction cross section. The (p, γ) reactions on the target nuclei ^{23}Mg, ^{27}Si, ^{31}S, ^{35}Ar, and ^{39}Ca (*yellow squares* in Fig. 1) have Q values in the range 0.5–2.0 MeV, and, consequently, the assumptions mentioned above are usually not valid. Therefore, it has been assumed in the literature (Champagne & Wiescher 1992; Rembges et al. 1997) that accurate stellar rates for these reactions are needed in order to predict quantitatively the nucleosynthesis in the mass region above $A = 20$. Furthermore, Rembges et al. (1997) recently proposed that the (p, γ) reactions on ^{23}Mg, ^{27}Si, ^{31}S, ^{35}Ar, and ^{39}Ca be measured directly at radioactive ion beam facilities.

In the present work we reevaluate the stellar rates for the (p, γ) reactions on ^{27}Si, ^{31}S, ^{35}Ar, and ^{39}Ca. The new reaction rates are based on the most recent experimental nuclear structure information. For ^{23}Mg$(p, \gamma)^{24}$Al, the available experimental information is not sufficient for a reliable determination of stellar rates. Results for this reaction, based on nuclear shell-model calculations, have been published elsewhere (Herndl et al. 1999). In the current literature, realistic uncertainties are usually not assigned to resonant reaction rates, and, consequently, little information is available regarding the reliability of the published results. In this work we compare nuclear structure properties (i.e., excitation energies, spectroscopic factors, proton partial widths, and γ-ray partial widths) of states belonging to the same isospin multiplet in order to estimate the uncertainties involved. Based on these results, we present for the first time reliable uncertainties of resonant reaction rates. Finally, we incorporate the present results into reaction network calculations and investigate astrophysical consequences of varying the reaction rates within their uncertainties. The present work specifically addresses the question if additional experimental work (e.g., direct cross section measurements with radioactive ion beams) is needed in order to improve the nuclear physics input information entering hydrodynamic simulations of specific astrophysical events.

A discussion of the procedures applied in the present work is given in § 2. Systematic comparisons of nuclear structure properties for nuclear states belonging to the same isospin multiplet are presented in §§ 2.2, 2.3, and 2.4. In § 2.5 we describe a method for estimating stellar reaction-rate uncertainties. Our recommended reaction rates with uncertainties are presented in § 3 together with a comparison to previous results. Consequences for the nucleosynthesis in novae and X-ray bursts are investigated in § 4, and a

summary and conclusions are given in § 5. Specific nuclear data and statistical methods used for determining the present results are discussed in Appendices A and B, respectively.

2. PROCEDURES

2.1. *Stellar Reaction Rates*

The total stellar rate for a (p, γ) reaction is determined by the sum of resonant and nonresonant contributions to the nuclear reaction mechanism.

For isolated narrow resonances, the reaction rate (in units of reactions s^{-1} mol^{-1} cm^3) as a function of stellar temperature T_9 (in units of GK) is given by (Fowler, Caughlan, & Zimmerman 1967)

$$N_A\langle\sigma v\rangle_r = 1.540 \times 10^{11}(\mu T_9)^{-3/2} \sum_i \omega\gamma_i e^{-11.605E_i/T_9} , \quad (1)$$

where the reduced mass μ is in amu and the center-of-mass energies E_i and strengths $\omega\gamma_i$ of the resonances are in MeV. The strength of a resonance in a (p, γ) reaction is defined by

$$\omega\gamma = \frac{2J+1}{(2j_p+1)(2j_T+1)} \frac{\Gamma_p\Gamma_\gamma}{\Gamma_p+\Gamma_\gamma} , \quad (2)$$

with J, j_p, and j_T as spins of the resonance, the projectile, and the target nucleus, respectively. The partial widths Γ_i describe the probability of decay or formation of the resonance through a particular channel i.

The nonresonant stellar rate for a (p, γ) reaction is usually determined by the contributions of the direct capture (DC) process into bound final states. The DC cross section varies smoothly with proton energy E and is usually converted into the astrophysical S-factor, defined by

$$S(E) = \sigma(E)Ee^{2\pi\eta} , \quad (3)$$

with η denoting the Sommerfeld parameter. If the S-factor can be approximated by the polynomial

$$S(E) = S(0) + ES'(0) + \tfrac{1}{2}E^2S''(0) , \quad (4)$$

the nonresonant reaction rates are obtained by using the relations (Fowler et al. 1967)

$$N_A\langle\sigma v\rangle_{nr} = 4.339 \times 10^8\tau^2 \frac{1}{\mu Z} e^{-\tau}S_{\rm eff} , \quad (5)$$

$$\tau = 4.248(Z^2\mu/T_9)^{1/3} , \quad (6)$$

$$S_{\rm eff} = S(0)\left[1 + \frac{5}{12\tau} + \frac{S'(0)}{S(0)}\left(E_0 + \frac{35}{36}kT\right) + \frac{1}{2}\frac{S''(0)}{S(0)}\left(E_0^2 + \frac{89}{36}E_0kT\right)\right]({\rm MeV} \times b) , \quad (7)$$

and

$$E_0 = 0.122(Z^2\mu T_9^2)^{1/3}({\rm MeV}) , \quad (8)$$

with Z the number of protons in the target nucleus. The cross section for the DC process can be estimated following the formalism described by Rolfs (1973). In the present work the radial wave functions for all bound final states are generated by using Woods-Saxon potentials. The well depths are chosen to reproduce the binding energies of the final states. The total DC cross section for the dominant E1 γ-ray transitions is given by the incoherent sum over orbital angular momenta ℓ_i and ℓ_f for all incoming and outgoing partial waves involved,

$$\sigma^{\rm DC}_{\rm total} = \sum_{\ell_i\ell_f} C^2S(\ell_f)\sigma^{\rm DC}_{\rm theor}(\ell_i,\ell_f) , \quad (9)$$

with $S(\ell_f)$ and C denoting the single-particle spectroscopic factor and the isospin Clebsch-Gordan coefficient, respectively.

2.2. *Nuclear Level Energies and Mirror Assignments*

The target nuclei ^{27}Si, ^{31}S, ^{35}Ar, and ^{39}Ca are short lived. Direct measurements of their proton-capture cross sections using radioactive ion beams have not yet been attempted. It is clear from the discussion in the previous subsection that the stellar reaction rates can be estimated empirically if appropriate nuclear structure information is available (i.e., resonance energies E_i, proton partial widths Γ_p, γ-ray partial widths Γ_γ, and spectroscopic factors S). However, only limited information is available for the corresponding proton-rich compound nuclei ^{28}P, ^{32}Cl, ^{36}K, and ^{40}Sc (Endt 1990, 1998). These nuclei have been investigated only through a restricted number of reactions with stable beams and targets. Energies E_X of excited states have been measured mainly by using the (^{3}He, t) charge-exchange reaction. The energies E_i of corresponding resonances in a (p, γ) reaction are then derived from the known reaction Q value (Audi & Wapstra 1995), $E_i = E_X - Q$. We have considered resonances with energies up to $E_i = 2$ MeV in order to estimate reaction rates for stellar temperatures $T_9 \leq 2$. Furthermore, the angular distributions measured in charge-exchange reactions are frequently sensitive to the value of the transferred orbital angular momentum L and therefore provide restrictions for level spins J and parities π.

For the nuclear states of interest in this work, no information is available on partial widths Γ_i and spectroscopic factors S. On the other hand, nuclear structure properties of the neutron-rich mirror nuclei ^{28}Al, ^{32}P, ^{36}Cl, and ^{40}K are well known (Endt 1990, 1998) because these nuclei are relatively easy to study experimentally using a variety of different nuclear reactions. Since nuclear forces are approximately charge independent, structure information on proton-rich nuclei can be adopted from corresponding information on neutron-rich nuclei.

The procedure just described requires an accurate prediction of mirror state correspondences. The assignments of mirror states in isospin triplets ($T = 1$) is mainly based on a comparison of experimental level energies E_X and J^π values (Endt 1990). Ambiguities frequently arise in cases where the Coulomb displacement energy between the mirror pair is relatively large. Mirror assignments are usually more reliable if Coulomb displacement energies can be estimated theoretically. (For recent applications of Coulomb shift calculations to levels of astrophysical importance, see Champagne, Brown, & Sherr 1993; Herndl et al. 1995; Iliadis et al. 1996.) In the present work we have predicted the excitation energies in the proton-rich nuclei of interest by using the isobaric multiplet mass equation (IMME). This equation, given by (Jänecke 1969; Benenson & Kashy 1979)

$$E(A, T, T_z) = a(A, T) + b(A, T)T_z + c(A, T)T_z^2 , \quad (10)$$

relates the energies (or masses) of the $2T + 1$ members of an isobaric multiplet. The z component T_z of the isospin ranges from $-T$ to $+T$. The coefficients a, b, and c are related to the scalar, vector, and isotensor Coulomb energies. For isobaric triplets ($T = 1$) equation (10) can be written in terms of excitation energies as

$$E_X(T_z = -1) = 2E_X(T_z = 0) - E_X(T_z = 1) + 2[c - c({\rm g.s.})] . \quad (11)$$

Consequently, the excitation energies of proton-rich ($T_z = -1$) nuclei can be estimated from experimentally well-known E_X values of the corresponding self-conjugate ($T_z = 0$) and neutron-rich ($T_z = 1$) nuclei. The term $[c - c(\text{g.s.})]$ reflects the difference in isotensor Coulomb energies between the isobaric triplet under consideration and the ground-state triplet.

The analog assignments are unambiguous for experimentally observed bound states in the proton-rich nuclei ^{24}Al, ^{28}P, ^{32}Cl, ^{36}K, and ^{40}Sc. For these levels, we have calculated excitation energies by using equation (11), where in first approximation the last term containing the c coefficients was neglected. The resulting differences $E_X^{exp} - E_X^{calc}$ are displayed in Figure 2 (*filled circles*). The average deviation amounts to $(E_X^{exp} - E_X^{calc})_{AV} = +17$ keV. For the average absolute deviation we find $|E_X^{exp} - E_X^{calc}|_{AV} = 50$ keV, which is close to typical uncertainties of excitation energies measured in (^{3}He, t) reaction studies (Endt 1990, 1998). The agreement is surprising and indicates that the c coefficients for the cases under consideration are approximately independent of excitation energy. Therefore, we have also used equation (11) without the last term for predicting excitation energies of unbound states in the proton-rich nuclei. Analog assignments have been found by (1) minimizing the difference between predicted and measured excitation energies in the proton-rich nuclei, and (2) matching the experimentally determined J^π values (or restrictions) for members of the same isospin triplet. The resulting energy differences $E_X^{exp} - E_X^{calc}$ for unbound states in ^{24}Al, ^{28}P, ^{32}Cl, ^{36}K, and ^{40}Sc are also displayed in Figure 2 (*open circles*). On average, the agreement is similar to the bound-state case. More detailed information regarding our analog assignments can be found in Appendix A.

An unsuccessful attempt was made in the present work to improve further the accuracy of E_X^{calc} values for the proton-rich nuclei of interest here by estimating the last term in equation (11) theoretically. The calculations are performed with the shell-model code OXBASH (Brown, Etchegoyen, & Rae 1985). The c coefficients are obtained from the empirical isospin nonconserving (INC) interaction of Ormand & Brown (1989) for the sd model space. The shell-model calculations also resulted in approximately constant c coefficients for bound and unbound states. However, the average absolute deviation $|E_X^{exp} - E_X^{calc}|_{AV}$ did not improve by taking the last term in equation (11) into account. This is surprising, since the INC matrix elements were obtained from fits to experimentally derived b and c coefficients.

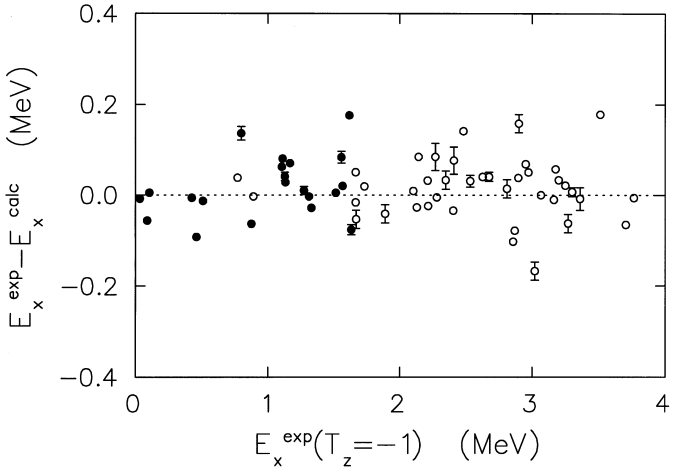

FIG. 2.—Differences between experimental and estimated excitation energies for bound (*filled circles*) and unbound (*open circles*) states in ^{24}Al, ^{28}P, ^{32}Cl, ^{36}K, and ^{40}Sc vs. experimental E_X^{exp} value. The E_X^{calc} values are estimated by using the isobaric multiplet mass equation (eq. [11]).

2.3. *Proton Partial Widths and Spectroscopic Factors*

Proton partial widths Γ_p are estimated by using the method described in Iliadis (1997), to which the reader is referred for details. In brief, values of Γ_p were computed according to the relation

$$\Gamma_p = 2 \frac{\hbar^2}{M_c a_c^2} P_c C^2 S_p \theta_{sp}^2 , \quad (12)$$

with M_c the reduced mass and P_c the penetrability of the Coulomb and centripetal barrier. The channel (or interaction) radius is usually written as $a_c = a_0(A^{1/3} + A_p^{1/3})$ with A and A_p the mass of the target and the projectile in amu, respectively. The dimensionless single-particle reduced width θ_{sp}^2 is given by

$$\theta_{sp}^2 = \frac{a_c}{2} \phi_\ell^2(a_c) , \quad (13)$$

where $\phi_\ell^2(a_c)$ denotes the square of the single-particle radial wave function of the ℓ orbit at the interaction radius a_c. We use the θ_{sp}^2 values of Iliadis (1997), which were obtained from radial wave functions generated by an optical-model potential. Values of $r_0 = 1.17$ fm and $a = 0.69$ fm were employed for the optical-model potential radius parameter and diffuseness, respectively. A justification for the choice of these values in the present work can be found in Iliadis (1997). In the current literature θ_{sp}^2 in equation (12) is usually set equal to unity. However, it is shown in Iliadis (1997) that this approximation introduces a significant error in the calculation of Γ_p. This error gives rise to an overestimate of the stellar reaction rates if they are influenced by the proton partial width of the compound-nucleus state in question.

For the proton spectroscopic factors S_p of the levels of interest here, we used the values for the neutron spectroscopic factors S_n of the corresponding states in the mirror nuclei. The S_n values were extracted from (d, p) neutron-transfer reaction data by applying the distorted-wave Born approximation (DWBA) theory (Glendenning 1983). It is well known that several uncertainties enter in a DWBA analysis, such as the proper values of the optical-model parameters, the parameters determining the bound-state radial wavefunctions of the transferred particle, finite-range and nonlocality effects, and contributions from multistep processes and compound nucleus formation and decay.

In order to estimate the reliability of measured single-particle spectroscopic factors we performed the following test (see Fig. 3). Since nuclear forces are approximately charge independent, we expect that single-particle (neutron or proton) spectroscopic factors for all components of the same isospin multiplet are approximately equal. For example, in order to calculate the stellar reaction rates for ^{27}Si(p, γ)^{28}P we need to know the S_p values for astrophysically important ^{28}P levels. Since this experimental information does not exist, we adopt the S_n values for the mirror states in ^{28}Al that were measured in ^{27}Al(d, p)^{28}Al reaction studies. However, these S_n values also have to be equal to S_p values of ^{28}Si ($T = 1$) analog states measured, for example, in ^{27}Al(^{3}He, d)^{28}Si reaction studies (Fig. 3).

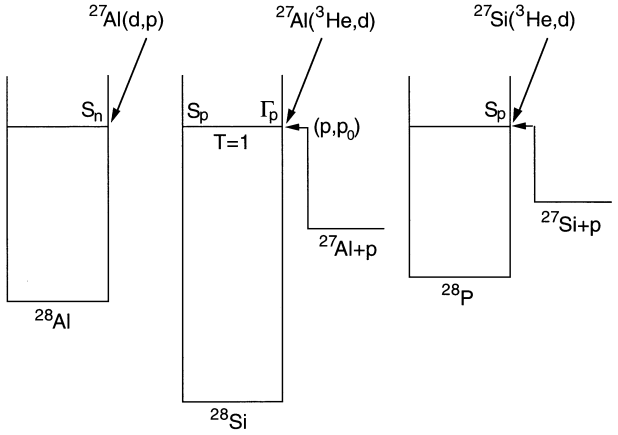

FIG. 3.—Isospin triplet states for the mass $A = 28$ system

Consequently, we have systematically compared spectroscopic factors from (d, p) and (^{3}He, d) reactions on ^{23}Na, ^{27}Al, ^{31}P, ^{35}Cl, and ^{39}K, populating states of the same isospin multiplet. This comparison represents a sensitive test since corresponding S_p and S_n values are extracted from different stripping reactions. We have found altogether 33 pairs of spectroscopic factors for which the required experimental information is available (Endt 1990; Endt & van der Leun 1978) and the resulting ratios S_n/S_p are shown in Figure 4*a*. Systematic trends and average scatter of the data are analyzed in the present work with the help of logarithmic means and logarithmic standard deviations, respectively. A discussion of these quantities from a statistical viewpoint is given in Appendix B. The logarithmic mean of the ratio S_n/S_p amounts to a factor of 0.94. The logarithmic standard deviation corresponds to a factor of 1.48. Therefore, we conclude that S_n values measured in the (d, p) reaction can indeed be used in equations (9) and (12) for the unknown S_p values, with an approximate uncertainty of a factor 1.5.

Strictly speaking, the above considerations do not provide a complete estimate for the reliability of our calculated proton partial widths Γ_p (eq. [12]). For example, uncertainties might exist for the optical-model parameters used for calculating the dimensionless single-particle reduced width θ_{sp}^2 (eq. [13]). Therefore, another quantitative test has been performed (Fig. 3). We used equation (12) together with S_n values measured in (d, p) reactions on ^{23}Na, ^{27}Al, and ^{31}P (Endt 1990; Endt & van der Leun 1978) in order to calculate proton partial widths Γ_p for $T = 1$ analog states in the $N = Z$ nuclei ^{24}Mg, ^{28}Si, and ^{32}S, respectively. The estimated values are then compared to experimental Γ_p values measured in proton elastic scattering experiments on ^{23}Na, ^{27}Al, and ^{31}P (Vanhoy et al. 1987; Nelson et al. 1984a, 1984b; Fang et al. 1988; Fang 1987). This comparison represents another sensitive test since the corresponding values for S_n and Γ_p^{exp} are extracted from independent measurements (nucleon transfer vs. resonant reaction). We found altogether 21 pairs of transitions for which the required information is available. No pairs were found for $T = 1$ analog states in $A = 36$ and 40 nuclei. The resulting ratios $\Gamma_p^{exp}/\Gamma_p^{calc}$ are displayed in Figure 4*b*. The logarithmic mean amounts to a factor of 1.03. The logarithmic standard deviation corresponds to a factor of 1.73. Therefore, we conclude that our method of calculating proton widths Γ_p by using equation (12) together with experimental S_n values provides reliable results to within a factor of about 1.7.

2.4. *Gamma-Ray Partial Widths*

The γ-ray partial widths Γ_γ for unbound levels of astrophysical interest are adopted from the corresponding bound states in the mirror nuclei. These Γ_γ values are derived from lifetimes measured by utilizing the Doppler shift attenuation method (DSAM). One might ask again how reliable this procedure is. Most of the γ-ray transitions of importance to the present work proceed between states of same parity ($\pi_i = \pi_f$) and isospin ($T_i = T_f$). For $\Delta T = 0$ transitions of magnetic dipole (M1) or electric quadrupole (E2) character the reduced transition probability B (which is proportional to the γ-ray transition strength) is given by (Brussaard & Glaudemans 1977)

$$B = (M_{IS} + T_z M_{IV})^2 , \qquad (14)$$

with M_{IS} and M_{IV} the isoscalar and isovector matrix elements, respectively. Although for corresponding γ-ray transitions in mirror nuclei the values for M_{IS} or M_{IV} are expected to be approximately equal, it is evident from equation (14) that the resulting transition strengths are generally not the same. However, it can be shown (Brussaard & Glaudemans 1977; Warburton & Weneser 1969) that for M1

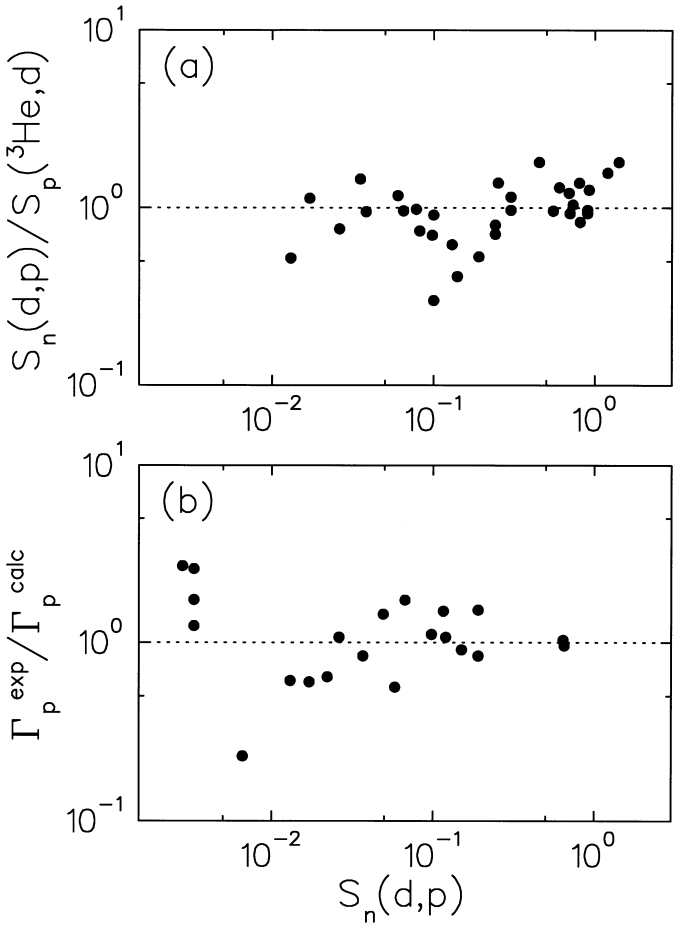

FIG. 4.—(*a*) Ratios of corresponding experimental neutron and proton spectroscopic factors for $A = 24$, 28, 32, 36, and 40 isospin triplet states, measured in (d, p) and (^{3}He, d) nucleon transfer reaction studies. (*b*) Ratios of corresponding experimental and estimated proton partial widths for $A = 24$, 28, and 32 isospin triplet states. The experimental and estimated Γ_p values are obtained from resonant elastic scattering experiments and from eq. (12), respectively.

(E2) γ-ray transitions the isovector (isoscalar) contribution dominates over the isoscalar (isovector) contribution. Therefore, we expect that γ-ray partial widths of corresponding transitions in mirror nuclei are of approximately equal strength.

As a quantitative test, we compared experimental γ-ray strengths for corresponding mirror transitions in nuclei with masses of $A = 21$–44. We disregarded all measured lifetimes with errors exceeding 30%. Strength ratios are corrected with a factor E_γ^{2L+1} if the γ-ray energies E_γ for corresponding transitions differ appreciably. Altogether, we found 44 pairs of transitions. The resulting ratios R of γ-ray strengths are shown in Figure 5.

The logarithmic mean amounts to a factor of 1.05, with a logarithmic standard deviation corresponding to a factor of 1.75. In conclusion, γ-ray partial widths Γ_γ for unbound levels in proton-rich nuclei can be estimated by using measured lifetimes of the corresponding bound mirror states in neutron-rich nuclei, with an uncertainty of a factor 1.7.

2.5. *Reaction-Rate Uncertainties*

For the reactions of interest in the present work, stellar rate uncertainties result from errors in resonance energies, proton partial widths, γ-ray partial widths, and single-particle spectroscopic factors (eqs. [1], [2], and [12]). Resonance energy errors derive from uncertainties of measured excitation energies and reaction Q values. Errors in Γ_p, Γ_γ, and S_p originate from experimental uncertainties of corresponding mirror-state properties and from the assumption of isospin symmetry. In this work we consider only randomly distributed errors. Systematic sources of uncertainties have been neglected. This assumption seems to be justified, since the logarithmic means (see Appendix B) for ratios of

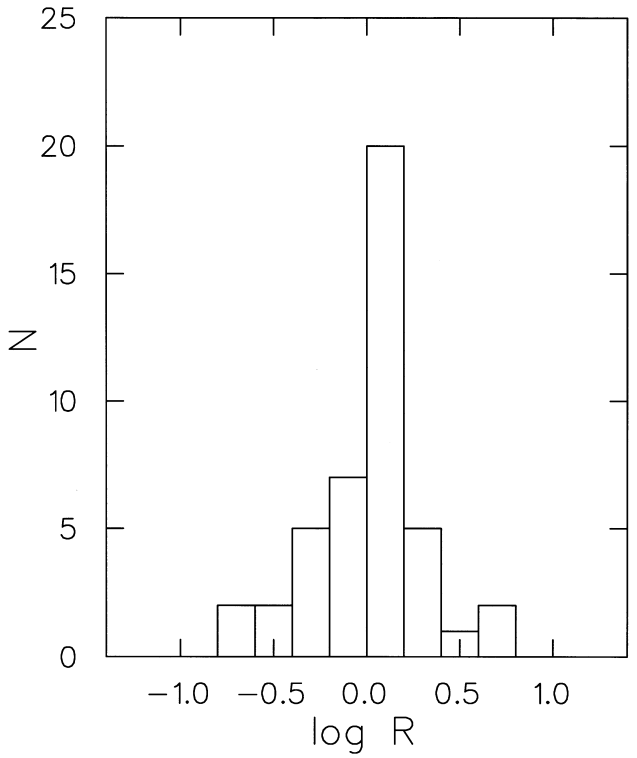

FIG. 5.—Ratios of γ-ray strengths for corresponding mirror transitions in nuclei with masses of $A = 21$–44; the quantity N denotes the number of ratios.

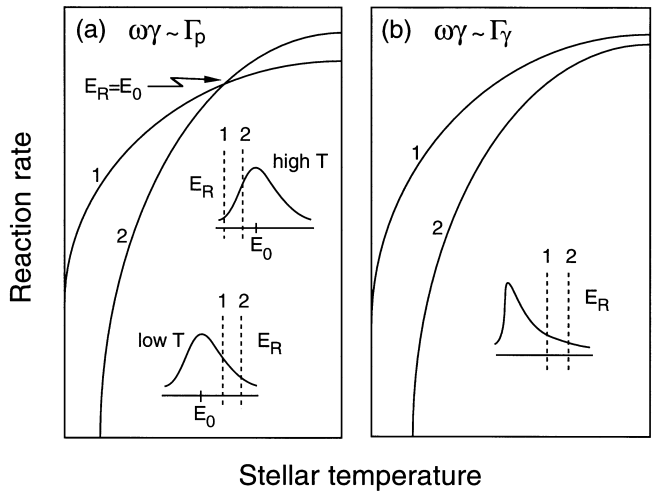

FIG. 6.—Influence of resonance energy variations on reaction-rate uncertainties in cases in which the resonance strength $\omega\gamma$ depends (*a*) only on the proton partial width and (*b*) only on the γ-ray partial width. The insets in (*a*) and (*b*) show the Gamow peak and Maxwell-Boltzmann distribution (*solid lines*), respectively. The dashed vertical lines indicate the location of a fictitious resonance.

particle widths, γ-ray widths, and single-particle spectroscopic factors (§§ 2.3 and 2.4) are within 6% of unity.

It is often stated in the literature that resonant reaction rates are most sensitive to variations in resonance energies, since this quantity enters exponentially in the reaction-rate expression (eq. [1]). However, this assumption represents an oversimplification. Instead, resonant reaction-rate errors are determined by the energy dependence of the Boltzmann factor (see eq. [1]), the penetrability through the Coulomb barrier (eq. [12]), and the relative magnitude of Γ_p and Γ_γ (eq. [2]). Figure 6 shows how a shift in resonance energy influences the resulting resonant reaction rates. Suppose that for a single resonance $\Gamma_p \ll \Gamma_\gamma$ such that the resonance strength $\omega\gamma$ is determined by Γ_p and is essentially independent of Γ_γ (Fig. 6*a*). If the resonance energy E_R is shifted up, the energy dependence of the Boltzmann factor tends to decrease the reaction rates. At the same time, the energy dependence of the Coulomb penetrability tends to increase the reaction rates. Both effects compensate each other to a degree that depends on the stellar temperature and the energy of the resonance. On the one hand, if the temperature is low and the Gamow peak maximum, E_0 given by equation (8), occurs at energies smaller than the resonance energy, then an increase in E_R causes a decrease of the resulting reaction rates, as shown in Figure 6*a*. On the other hand, at high stellar temperatures at which the Gamow peak maximum E_0 occurs at higher energies than the resonance, an increase in E_R causes an increase of the reaction rates. Clearly, a temperature region exists where the energy dependences of Boltzmann factor and Coulomb penetrability cancel each other approximately. More precisely, resonant reaction rates are insensitive to variations in resonance energies for stellar temperatures at which the resonance energy is near the Gamow peak location, i.e., $E_R \approx E_0$. Numerical tests show that this result is nearly independent of the transferred orbital angular momentum ℓ.

This effect is often overlooked in the literature. Suppose, for example, that both a resonance strength of $\omega\gamma = 8 \times 10^{-8}$ eV ($\pm 5\%$) and a proton spectroscopic

TABLE 1

RESONANCE PARAMETERS FOR THE REACTION $^{27}Si(p, \gamma)^{28}P$

$E_x(^{28}P)$[a] (keV)	$E_x(^{28}Al)$ (keV)	J_n^π	E_R^{cm}[b] (keV)	Γ_p (eV)	Γ_γ (eV)	$\omega\gamma$ (eV)
2104 ± 1.....	2139	2_3^+	38 ± 4	3.1×10^{-21}	6.0×10^{-2}	1.3×10^{-21}
2143 ± 5.....	2201	1_3^+	77 ± 6	5.1×10^{-14}	1.1×10^{-2}	1.3×10^{-14}
2216 ± 5.....	2272	4_1^+	150 ± 6	4.0×10^{-8}	2.1×10^{-2}	3.0×10^{-8}
2406 ± 5.....	2486	2_4^+	340 ± 6	3.5×10^{-2}	6.9×10^{-3}	2.4×10^{-3}
2483 ± 5.....	2582	5_1^+	417 ± 6	1.7×10^{-2}	1.4×10^{-3}	1.2×10^{-3}
2628 ± 5.....	2656	4_2^+	562 ± 6	1.4×10^{0}	2.1×10^{-2}	1.5×10^{-2}
2857 ± 5.....	3012	0_2^+	791 ± 6	7.2×10^{0}	1.0×10^{-2}[c]	8.4×10^{-4}
2896 ± 5.....	2988	3_3^+	830 ± 6	$>1.4 \times 10^{0}$[d]	7.3×10^{-3}	4.2×10^{-3}
2973 ± 5.....	3105	1_4^+	907 ± 6	1.9×10^{1}	3.1×10^{-2}	7.8×10^{-3}
3164 ± 5.....	3296	3_4^+	1098 ± 6	3.1×10^{2}	6.0×10^{-2}	3.5×10^{-2}
3200 ± 5.....	3347	2_5^+	1134 ± 6	4.6×10^{2}	7.3×10^{-2}	3.0×10^{-2}
3250 ± 5.....	3465	4_1^-	1184 ± 6	1.3×10^{3}	1.0×10^{-2}	7.7×10^{-3}
3512 ± 5.....	3542	1_5^+	1446 ± 6	1.2×10^{2}	8.3×10^{-2}[c]	2.1×10^{-2}

[a] Experimental values, adopted from Endt 1998.
[b] Calculated from first column using $Q_{p\gamma} = 2065.6 \pm 3.7$ keV (Audi & Wapstra 1995).
[c] Shell-model estimate for ^{28}Al mirror state (Endt & Booten 1993).
[d] Calculated by using $S_{\ell=2}$ component only and, therefore, represents a lower limit.

factor of $S_p = 0.5^{+0.5}_{-0.25}$ have been measured for a fictitious s-wave resonance at $E_R^{cm} = 180 \pm 10$ keV in $^{35}Ar(p, \gamma)^{36}K$. It is easily shown from equations (1) and (12) that for a temperature of $T_9 = 0.1$ (i.e., where $E_0 = E_R^{cm}$) the resulting reaction rates are uncertain by a factor of 3 (or 2) if they are calculated from the measured value for $\omega\gamma$ (or S_p). Therefore, one might conclude that in certain situations experimental determinations of spectroscopic factors yield more reliable reaction rates than resonance strength measurements, even if the error for S_p is much larger than the uncertainty in $\omega\gamma$.

If, instead, the condition $\Gamma_\gamma \ll \Gamma_p$ is fulfilled, the resonance strength $\omega\gamma$ is determined by Γ_γ. Since the value of Γ_p has no influence on the reaction rates, the concept of a Gamow peak is not useful. In this case, an upward shift in resonance energy E_R decreases the reaction rates for all stellar temperatures because of the energy dependence of the Boltzmann factor, as shown in Figure 6*b*. The energy dependence of Γ_γ is usually small and can be neglected here.

In general, several resonances of different energies will contribute to the reaction rates. At low stellar temperatures, the reaction rates are determined by low-energy resonances with $\omega\gamma \approx \Gamma_p$. Typical uncertainties in resonance energies can cause large errors in reaction rates because of the strong energy dependence of the Coulomb penetrability. At high stellar temperatures, the reaction rates are most likely dominated by higher lying resonances with $\omega\gamma \approx \Gamma_\gamma$. Typical uncertainties of E_R values will cause relatively small errors in reaction rates because of the weak energy dependence of the Boltzmann factor at high energies.

In the present work, a program has been written in order to estimate random errors of reaction rates. Resonance energies E_R are varied within their assigned uncertainties (fourth column in Tables 1, 2, 3, and 4) explicitly taking the energy dependence of the corresponding proton partial widths Γ_p into account (eq. [12]). Uncertainties in γ-ray partial widths Γ_γ and proton spectroscopic factors S_p are additional sources of errors. These quantities, for which we

TABLE 2

RESONANCE PARAMETERS FOR THE REACTION $^{31}S(p, \gamma)^{32}Cl$

$E_x(^{32}Cl)$[a] (keV)	$E_x(^{32}P)$ (keV)	J_n^π	E_R^{cm}[b] (keV)	Γ_p (eV)	Γ_γ (eV)	$\omega\gamma$ (eV)
1733 ± 2.....	1755	3_1^+	158 ± 7	2.6×10^{-11}	1.1×10^{-3}	4.6×10^{-11}
2130 ± 3.....	2177	3_2^+	555 ± 8	8.1×10^{-4}	8.6×10^{-3}	1.3×10^{-3}
2212 ± 3.....	2230	1_3^+	637 ± 8	4.1×10^{0}	1.6×10^{-2}	1.2×10^{-2}
2281 ± 3.....	2218	2_3^+	706 ± 8	1.9×10^{-1}	2.7×10^{-3}	3.4×10^{-3}
2574[c].....	2740	1_4^+	999	5.1×10^{0}	3.3×10^{-2}	2.4×10^{-2}
2676 ± 10.....	2658	2_4^+	1101 ± 12	4.9×10^{0}	5.5×10^{-2}	6.8×10^{-2}
2869 ± 5.....	3005	3_3^+	1294 ± 9	1.2×10^{1}	6.5×10^{-3}	1.1×10^{-2}
2952 ± 5.....	3264	2_1^-	1377 ± 9	2.7×10^{3}	4.0×10^{-3}	5.0×10^{-3}
3067 ± 5.....	3443	4_1^-	1492 ± 9	5.4×10^{1}	1.7×10^{-3}	3.8×10^{-3}
3177 ± 5.....	3320	3_1^-	1602 ± 9	5.6×10^{1}	2.4×10^{-3}	4.2×10^{-3}
3301 ± 10.....	3444	2_5^+	1726 ± 12	...[d]	1.7×10^{-2}	$<2.2 \times 10^{-2}$
3397[c].....	3149	4_1^+	1822	...[d]	1.1×10^{-3}	$<2.5 \times 10^{-3}$

[a] Experimental values, adopted from Endt 1998.
[b] Calculated from first column using $Q_{p\gamma} = 1574.7 \pm 6.9$ keV (Audi & Wapstra 1995).
[c] State has not been observed experimentally. The E_x value is estimated by using the IMME (eq. [11]). The estimated uncertainty is 50 keV (§ 2.2).
[d] Value is not estimated, since the spectroscopic factor S of the ^{32}P mirror state has not been measured. The upper limit for $\omega\gamma$ is calculated with $\omega\gamma \leq \omega\Gamma_\gamma$ (since $\Gamma_p/\Gamma \leq 1$).

TABLE 3

RESONANCE PARAMETERS FOR THE REACTION $^{35}Ar(p, \gamma)^{36}K$

$E_X(^{36}K)$[a] (keV)	$E_X(^{36}Cl)$ (keV)	J_n^π	E_R^{cmb} (keV)	Γ_p (eV)	Γ_γ (eV)	$\omega\gamma$ (eV)
1670 ± 20.....	1951	2_1^-	4 ± 21	3.2×10^{-109}	2.7×10^{-4}	2.0×10^{-109}
1890 ± 20.....	1959	2_2^+	224 ± 21	5.7×10^{-7}	1.0×10^{-2}	3.6×10^{-7}
2270 ± 30.....	2468	3_1^-	604 ± 31	4.2×10^{-1}	4.7×10^{-4}	4.1×10^{-4}
2410 ± 30.....	2492	2_3^+	744 ± 31	2.5×10^{0}	1.1×10^{-2}	6.8×10^{-3}

[a] Experimental values, adopted from Endt 1998.
[b] Calculated from first column using $Q_{p\gamma} = 1665.8 \pm 7.8$ keV (Audi & Wapstra 1995).

TABLE 4

RESONANCE PARAMETERS FOR THE REACTION $^{39}Ca(p, \gamma)^{40}Sc$

$E_X(^{40}Sc)$[a] (keV)	$E_X(^{40}K)$ (keV)	J_n^π	E_R^{cmb} (keV)	Γ_p (eV)	Γ_γ (eV)	$\omega\gamma$ (eV)
772 ± 2.....	800	2_1^-	233 ± 5	2.0×10^{-9}	1.6×10^{-3}	1.2×10^{-9}
892 ± 2.....	891	5_1^-	353 ± 5	3.0×10^{-7}	5.3×10^{-4}	4.2×10^{-7}
1667 ± 4.....	2047	2_2^-	1128 ± 6	2.2×10^{2}	1.3×10^{-3}	8.4×10^{-4}
1667 ± 4.....	2103	1_1^-	1128 ± 6	3.0×10^{2}	8.8×10^{-4}	3.3×10^{-4}

[a] Experimental values, adopted from Endt 1998.
[b] Calculated from first column using $Q_{p\gamma} = 539.1 \pm 4.5$ keV (Audi & Wapstra 1995).

assumed an error of a factor 1.7 (§§ 2.3 and 2.4), are varied independently of the resonance energies. Upper and lower limits of resonant reaction rates are added to direct capture reaction rates. For the DC contribution we assumed that the uncertainties arise mainly from errors in proton spectroscopic factors S_p (eq. [9]). The resulting upper and lower limits on total reaction rates are discussed together with our recommended rates in the following section.

3. RECOMMENDED REACTION RATES AND UNCERTAINTIES

The parameters used for calculating resonant reaction rates are presented in Tables 1, 2, 3, and 4. Astrophysical S-factors for the direct capture contributions are given in Table 5. Our recommended total reaction rates, which are valid for stellar temperatures of $T_9 = 0.01$–2.0, are listed in Table 6. The present reaction rates are compared to previous results in Figure 7. Reaction-rate uncertainties are displayed in Figure 8. In the following, we discuss briefly the results for each reaction considered separately. More details are given in Appendix A.

The $^{27}Si(p, \gamma)^{28}P$ reaction rates are determined by resonances with energies of $E_R \leq 562$ keV for all temperatures of interest here ($T_9 = 0.01$–2). Contributions of higher lying resonances and the direct capture process into seven ^{28}P bound states (Table 5) are negligible. The present reaction rates agree with the previous estimate (Wiescher et al. 1986) to within a factor of 2 for temperatures $T_9 > 0.07$ (Fig. 7*a*). For lower temperatures, $T_9 = 0.01$–0.07, the present reaction rates deviate by up to 6 orders of magnitude from the results of Wiescher et al. (1986), in which contributions of the low-energy resonance at $E_R = 38$ keV (Table 1) were neglected. The ratio of upper and lower limits on the total reaction rates amounts to a factor of three at temperatures $T_9 = 0.03$–2.0 (Fig. 8*a*) and is determined by random errors of the quantities S_p and Γ_γ. The ratio reaches a maximum value of a factor 12 at $T_9 = 0.02$. However, at these low temperatures the $^{27}Si + p$ reaction rates are astrophysically unimportant since the lifetime of ^{27}Si versus destruction by proton capture exceeds the lifetime of the competing β-decay by many orders of magnitude for densities $\rho \leq 10^7$ g cm^{-3} encountered in explosive hydrogen-burning scenarios.

The $^{31}S(p, \gamma)^{32}Cl$ reaction rates are determined by resonances with energies $E_R \leq 1101$ keV for temperatures $T_9 = 0.04$–2. Contributions of higher lying resonances are negligible. The direct capture process into five bound ^{32}Cl states (Table 5) determines the total reaction rates for temperatures below $T_9 = 0.03$. The present reaction rates differ from previous results (Vouzoukas et al. 1994) by a factor of 4 in the temperature range $T_9 = 0.1$–0.3 (Fig. 7*b*). This deviation arises from the use of our improved method of calcu-

TABLE 5

EXPANSION COEFFICIENTS OF THE TOTAL S-FACTOR FOR DIRECT CAPTURE INTO ALL BOUND FINAL STATES[a]

Reaction	S(0) (MeV × b)	S′(0) (b)	S″(0) (b/MeV)
$^{27}Si(p, \gamma)^{28}P$.....	7.87×10^{-2}	-1.54×10^{-2}	1.00×10^{-2}
$^{31}S(p, \gamma)^{32}Cl$	7.51×10^{-2}	-3.46×10^{-2}	3.10×10^{-2}
$^{35}Ar(p, \gamma)^{36}K$	1.24×10^{-1}	-8.66×10^{-2}	9.96×10^{-2}
$^{39}Ca(p, \gamma)^{40}Sc$.....	3.75×10^{-2}	1.58×10^{-2}	0

[a] The S-factor parameterizations are valid for bombarding energies of $E_p \leq 1$ MeV. The total S-factor, given by eq. (4), has been calculated by using eqs. (3) and (9) (see § 2).

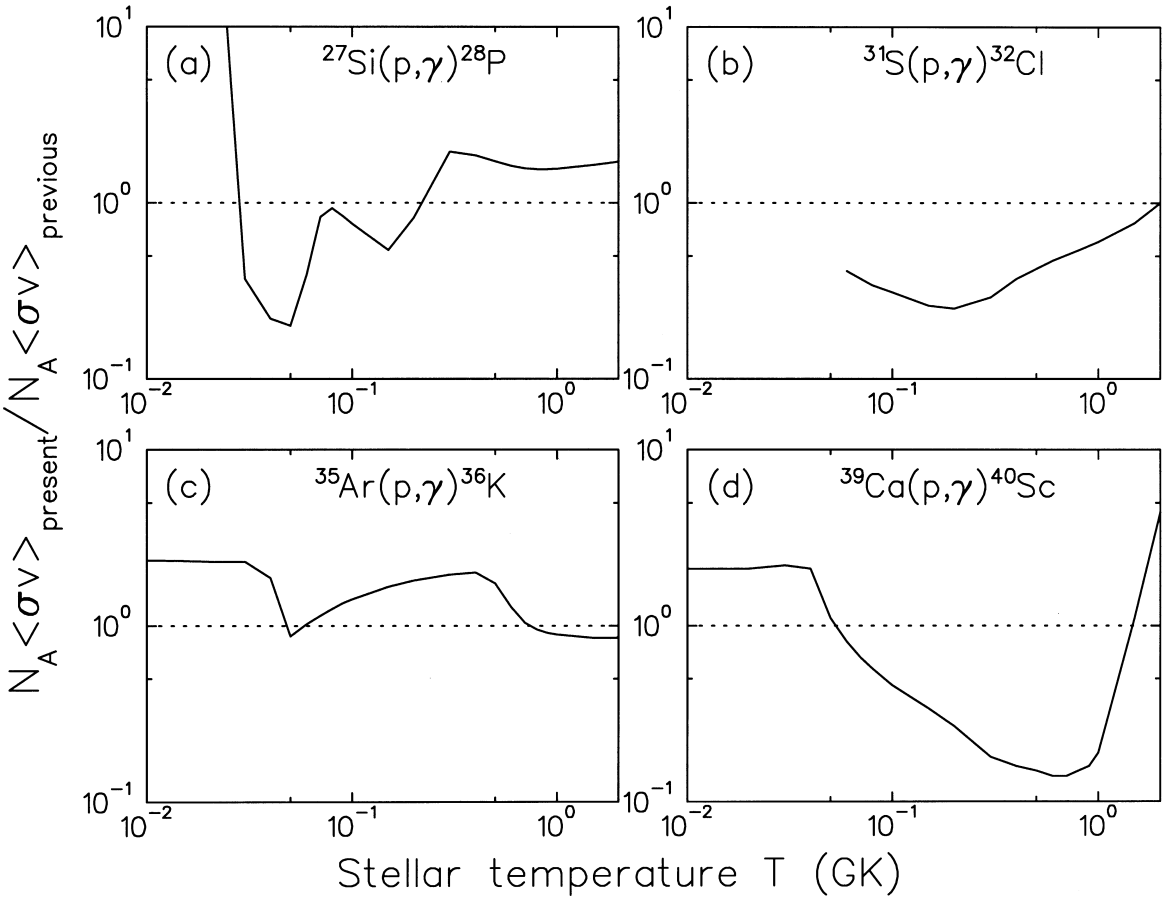

FIG. 7.—Ratios of our recommended reaction rates to previous results (see text) vs. stellar temperature

lating proton partial widths Γ_p (see § 2.3). The ratio of upper and lower limits on the total reaction rates amounts to a factor of 3 at temperatures $T_9 < 0.03$ and $T_9 > 0.05$ (Fig. 8*b*) and, again, is determined by random errors of S_p and Γ_γ. The ratio reaches a maximum value of 7 at $T_9 \approx 0.04$. However, for reasons outlined in the previous paragraph, the $^{31}S + p$ reaction rates are of minor astrophysical importance at such low temperatures.

TABLE 6

RECOMMENDED STELLAR REACTION RATES $N_A\langle\sigma v\rangle$ (cm^3 mol^{-1} s^{-1})

T_9 (GK)	^{27}Si(p, γ)^{28}P	^{31}S(p, γ)^{32}Cl	^{35}Ar(p, γ)^{36}K	^{39}Ca(p, γ)^{40}Sc
0.01	9.1×10^{-33}	5.1×10^{-44}	3.0×10^{-48}	4.9×10^{-53}
0.015.....	1.4×10^{-26}	2.4×10^{-37}	5.2×10^{-41}	3.0×10^{-45}
0.02	1.5×10^{-23}	4.0×10^{-33}	1.9×10^{-36}	2.5×10^{-40}
0.03	5.3×10^{-20}	7.6×10^{-28}	1.0×10^{-30}	3.7×10^{-34}
0.04	4.6×10^{-17}	1.2×10^{-23}	4.5×10^{-27}	2.9×10^{-30}
0.05	3.2×10^{-15}	7.8×10^{-20}	1.3×10^{-22}	6.1×10^{-26}
0.06	1.2×10^{-13}	2.5×10^{-17}	5.8×10^{-19}	3.7×10^{-22}
0.07	4.2×10^{-12}	1.6×10^{-15}	2.2×10^{-16}	1.8×10^{-19}
0.08	7.4×10^{-11}	3.5×10^{-14}	1.9×10^{-14}	1.9×10^{-17}
0.09	6.9×10^{-10}	3.7×10^{-13}	5.9×10^{-13}	6.7×10^{-16}
0.1	4.1×10^{-9}	2.5×10^{-12}	9.1×10^{-12}	1.1×10^{-14}
0.15	7.7×10^{-7}	6.1×10^{-10}	2.9×10^{-8}	5.3×10^{-11}
0.2	2.1×10^{-5}	8.6×10^{-9}	1.4×10^{-6}	4.0×10^{-9}
0.3	4.8×10^{-3}	9.4×10^{-7}	6.0×10^{-5}	6.3×10^{-7}
0.4	8.5×10^{-2}	1.6×10^{-4}	3.5×10^{-4}	1.0×10^{-5}
0.5	4.6×10^{-1}	3.6×10^{-3}	1.1×10^{-3}	5.5×10^{-5}
0.6	1.4×10^{0}	2.9×10^{-2}	4.1×10^{-3}	1.6×10^{-4}
0.7	3.1×10^{0}	1.3×10^{-1}	1.5×10^{-2}	3.4×10^{-4}
0.8	5.5×10^{0}	3.8×10^{-1}	4.9×10^{-2}	5.9×10^{-4}
0.9	8.8×10^{0}	8.9×10^{-1}	1.2×10^{-1}	9.5×10^{-4}
1.0	1.3×10^{1}	1.7×10^{0}	2.6×10^{-1}	1.5×10^{-3}
1.5	3.9×10^{1}	1.2×10^{1}	2.2×10^{0}	2.0×10^{-2}
2.0	7.0×10^{1}	3.4×10^{1}	5.9×10^{0}	1.1×10^{-1}

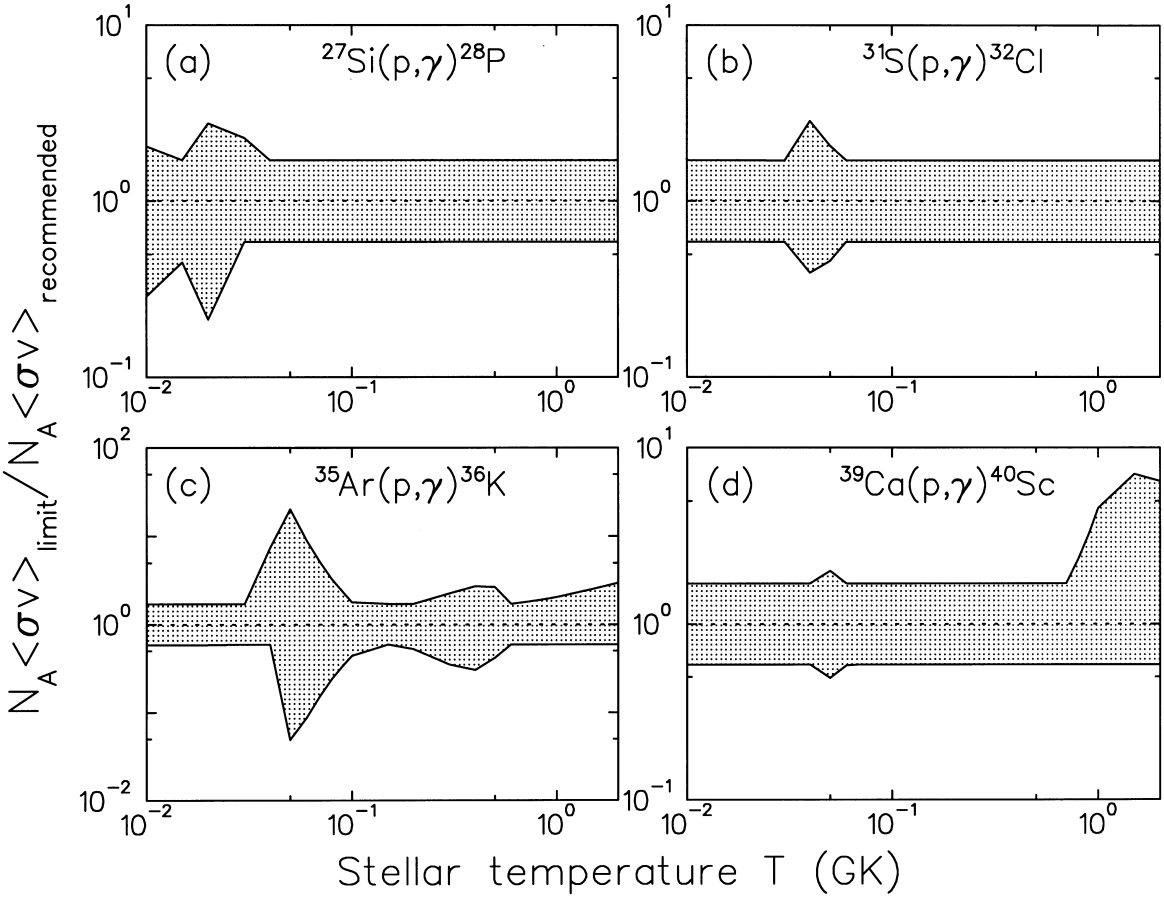

FIG. 8.—Solid lines represent 1 σ upper and lower limits of stellar reaction rates normalized to our recommended rates. Shaded areas indicate the present estimate of reaction-rate uncertainties.

For temperatures of $T_9 \geq 0.05$, the ^{35}Ar(p, γ)^{36}K reaction rates are dominated by narrow resonances with energies $E_R = 224$–744 keV. The direct capture process into four bound ^{36}K states (Table 5) dominates the reaction rates at lower temperatures. The present reaction rates agree to within a factor of 2 (Fig. 7*c*) with previous results (Herndl et al. 1995), which are based on shell-model estimates of proton and γ-ray partial widths. The ratio of upper and lower reaction-rate limits reaches maximum values of 400, 9, and 5, at temperatures $T_9 \approx 0.05$, 0.4, and 2.0, respectively (Fig. 8*c*). The first uncertainty occurring at low temperatures is astrophysically unimportant. The latter two uncertainties arise mainly from random errors in resonance energies E_R and the possible contributions of higher lying resonances not listed in Table 3, respectively (see Appendix A3).

The rates for the ^{39}Ca(p, γ)^{40}Sc reaction are determined for temperatures $T_9 \geq 0.05$ by resonances with energies $E_R \leq 1128$ keV. The direct capture process into two bound ^{40}Sc states (Table 5) dominates the reaction rates at lower temperatures. The present reaction rates differ from previous results (Wiescher & Görres 1989) by a factor of 7 at temperatures $T_9 = 0.3$–0.9 (Fig. 7*d*), mainly because of the application of our improved method for calculating proton partial widths (§ 2.3). The ratio of upper and lower reaction-rate limits reaches maxima of factors 4 and 11 at temperatures $T_9 \approx 0.05$ and ≥ 1.0, respectively (Fig. 8*d*). The latter uncertainty arises from the possible contributions of higher lying resonances not listed in Table 4 (Appendix A4), while the first uncertainty at low temperatures is of no astrophysical relevance.

4. REACTION NETWORK CALCULATIONS

4.1. *Procedure*

Here we present the results of reaction network calculations, in order to investigate the astrophysical implications of our new reaction rates. In addition, we investigate the effect of varying the new reaction rates within their uncertainties. If either the energy generation or element production is found to be sensitive to rate variations, one may conclude that further experimental and theoretical work is needed in order to estimate more accurate reaction rates.

The time-integrated net abundance flow F_{ij} between two specific nuclei i and j is given by the expression

$$F_{ij} = \int \left[\frac{dY_i(i \rightarrow j)}{dt} - \frac{dY_j(j \rightarrow i)}{dt} \right] dt \, , \qquad (15)$$

with $dY_i/dt(i \rightarrow j)$ the partial rate of change of the isotopic abundance $Y_i = X_i/A_i$, induced by reactions converting nucleus i to j. The total rate of change of the abundance of a particular nucleus i is determined by the rate equation

$$\frac{dY_i}{dt} = \sum_j \lambda_j Y_j + \sum_{j,\,k} \rho N_A \langle \sigma v \rangle_{jk} Y_j Y_k \, , \qquad (16)$$

where the sums include all nuclear transformations creating or destroying nucleus i. The first term in equation (16) con-

tains the decay constant λ_j of nucleus j into nucleus i and describes β-decays and photodisintegrations. The second term represents reactions between two nuclei, j and k. Three-particle interactions are not shown in equation (16) but are also taken into account in our calculations. The resulting system of coupled differential equations is solved at each integration time step τ by using the method described in Wagoner (1969) and Prantzos, Arnould, & Arcoragi (1987). Time steps are chosen such that all abundances of nuclei j with $Y_j \geq Y_{\rm min}$ vary by less than 25% over the interval τ. The value for $Y_{\rm min}$ is typically set between 10^{-14} and 10^{-10}.

The nuclear reaction network consists of 394 different nuclei from hydrogen to yttrium between the proton drip line and the stable isotopes. It involves 3933 nuclear processes, including weak interactions, reactions of type (p, γ), (p, α), (α, γ), etc., and corresponding reverse reactions. The latter are calculated from the forward reaction rates by using the principle of time-reversal invariance (Fowler et al. 1967). Most of the thermonuclear reaction rates are adopted from Thielemann's database REACLIB[1]. For several proton-induced reactions, recently published stellar rates are taken into account in our network calculations. These reactions and the corresponding references are listed in Table 7, together with the (p, γ) reactions discussed in the present work.

In addition to the information given above, the network calculations require assumptions regarding temperature, density, and total burning time characteristic of the stellar event under consideration. In the present work we investigate the nucleosynthesis in novae and X-ray bursts. In both cases we have used temperature and density profiles obtained from recent hydrodynamical simulations of accreting white dwarfs and neutron stars.

4.2. *Nucleosynthesis in Novae*

A classical nova is believed to be caused by the accretion of hydrogen-rich material onto a white dwarf in a close binary system. Underlying white dwarf material is dredged up into the accreted hydrogen layer. A subsequent thermonuclear runaway occurs on the surface of the white dwarf until a significant fraction of material, enriched in products of hydrogen burning, is ejected into the interstellar medium. For a recent review, see Gehrz et al. (1998). Observations of the elements Ne, Na, Al, Mg, S, and Ar in certain nova ejecta have led to the important discovery of a new nova class, so-called ONeMg or "neon" novae. The observed heavy-element enrichments can be explained by assuming an underlying ONeMg white dwarf, i.e., a white dwarf resulting from cores of massive stars that have experienced core carbon burning. In this scenario initially abundant O, Ne, and Mg isotopes are mixed into the hydrogen-burning envelope and are converted by the rp-process (§ 1) to heavier nuclei with masses $A = 20$–40. It has also been suggested (Weiss & Truran 1990) that ONeMg novae may represent an important source of ^{22}Na and ^{26}Al in the Galaxy.

In the present work the nucleosynthesis in ONeMg novae is studied by using the nuclear reaction network described in § 4.1. The calculations are performed with temperature and density profiles obtained from recent hydrodynamical studies (Politano et al. 1995) of thermonuclear runaways initiated by accretion onto white dwarfs with masses of 1.25 and 1.35 $M_\odot$. These two sequences reach peak temperatures of $T_9 = 0.29$ and 0.35, respectively, in the deepest hydrogen-rich zone. The nucleosynthesis is followed over time periods of several days until temperatures and densities drop to values of about $T_9 = 0.05$ and $\rho = 1$ g cm^{-3}, respectively, at which no further important nuclear reactions occur. For the initial isotopic abundances we adopt the results presented in Table 1 of Politano et al. (1995), which are derived from carbon-burning nucleosynthesis calculations (Arnett & Truran 1969). The initial material consists to 99.7% (by mass) of ^{1}H, ^{4}He, ^{16}O, ^{20}Ne, and ^{24}Mg.

It is not our intention to reproduce quantitatively the element abundances observed in nova ejecta. Realistic studies of nova nucleosynthesis require the use of an extended nuclear reaction network that is directly coupled to hydrodynamic evolutionary models. The reason is, as pointed out in Starrfield et al. (1993), that convective mixing carries material from the hydrogen-burning region to the surface on short timescales. This will cause an increase in

[1] Available at http://isotopes.lbl.gov/isotopes/astro/friedel.html.

TABLE 7

UPDATED STELLAR RATES IN REACTION NETWORK[a]

Reaction	Reference	Reaction	Reference
^{13}N$(p, \gamma)^{14}$O	Decrock et al. 1993	^{31}P$(p, \alpha)^{28}$Si	Iliadis et al. 1993[b]
^{22}Na$(p, \gamma)^{23}$Mg	Stegmüller et al. 1996	^{31}S$(p, \gamma)^{32}$Cl	present work
^{23}Mg$(p, \gamma)^{24}$Al	Herndl et al. 1998	^{32}S$(p, \gamma)^{33}$Cl	Iliadis et al. 1992a[c]
^{25}Mg$(p, \gamma)^{26}$Al^g	Iliadis et al. 1996	^{35}Cl$(p, \gamma)^{32}$S	Iliadis et al. 1994[b]
^{25}Mg$(p, \gamma)^{26}$Al^m	Iliadis et al. 1996	^{35}Ar$(p, \gamma)^{36}$K	present work
^{25}Al$(p, \gamma)^{26}$Si	Iliadis et al. 1996	^{36}Ar$(p, \gamma)^{37}$K	Iliadis et al. 1992b
^{26}Al$^g(p, \gamma)^{27}$Si	Champagne et al. 1993[d]	^{39}Ca$(p, \gamma)^{40}$Sc	present work
^{27}Si$(p, \gamma)^{28}$P	present work	^{40}Ca$(p, \gamma)^{41}$Sc	Wiescher & Görres 1989[e]
^{28}Si$(p, \gamma)^{29}$P	Graff et al. 1990	^{56}Ni$(p, \gamma)^{57}$Cu	Rehm et al. 1998[f]
^{31}P$(p, \gamma)^{32}$S	Iliadis et al. 1993		

[a] Stellar rates for all other reactions are adopted from the library REACLIB (see § 4.1).

[b] With additional information from Ross et al. 1995.

[c] In the present work an improved value of $\omega\gamma(E_R = 77$ keV$) = 1.0 \times 10^{-17}$ eV has been used (eq. [12]).

[d] With additional information from Vogelaar 1989.

[e] In the present work the correct value of $\omega\gamma(E_R = 647\ ) = 1.8\ \times 10^{-3}$ eV has been used (P. M. Endt 1997, private communication).

[f] With additional information from Zhou et al. 1996.

ejected abundances of nuclei that are easily destroyed if they are not carried to higher and cooler layers. Results of such studies have been reported recently (Politano et al. 1995; Starrfield et al. 1998). Instead, we are investigating the impact of our recommended reaction rates and their uncertainties on final abundances. For the purpose of the present work, the use of one-zone nucleosynthesis models should therefore be appropriate.

Time-integrated net abundance flows F_{ij}, obtained in this work by using our recommended reaction rates (Tables 6 and 7) and temperature-density profiles for the 1.25 $M_\odot$ and 1.35 $M_\odot$ sequences (Politano et al. 1995), are displayed in Figure 9. The strength of the abundance flows is represented by lines of different thickness (see the legend to Fig. 9 for an explanation). Our final isotopic abundances are listed in Table 8. The results for the two different nova sequences show several common features: (1) initially abundant ^{16}O nuclei are redistributed through the HCNO cycles, (2) initially present ^{20}Ne nuclei are processed through the NeNa cycle, and (3) both of the abundant isotopes ^{20}Ne and ^{24}Mg are converted to heavier mass nuclei. Figure 9 and Table 8 also demonstrate an important difference. The main abundance flow for the 1.25 $M_\odot$ sequence stops at ^{32}S, primarily because of the small rate for the ^{32}S(p, γ)^{33}Cl reaction (see Table 7). On the other hand, a significant abundance flow reaches the Cl and Ar isotopes for the 1.35 $M_\odot$ sequence, which achieves a higher peak temperature. These results reproduce qualitatively observed heavy-element enrichments in ONeMg nova ejecta and are consistent with previous conclusions (Politano et al. 1995; Starrfield et al. 1998). The total amount of energy released by nuclear reactions and decays is $\epsilon_{\rm nuc} = 8.2 \times 10^{17}$ ergs g^{-1} (1.3×10^{18} ergs g^{-1}) for the 1.25 $M_\odot$ (1.35 $M_\odot$) sequence. In the following, we concentrate on the role of proton-capture reactions that are of primary interest in the present work.

Time evolutions of ^{27}Si, ^{31}S, ^{35}Ar, and ^{39}Ca abundances for the two nova sequences considered are displayed in Figure 10. The main abundance flow reaches ^{27}Si, which subsequently is depleted by both the (p, γ) reaction and the competing β-decay. The main flow continues to ^{31}S, which is depleted by the subsequent β-decay. As mentioned above, only minor flows extend beyond ^{32}S in the 1.25 $M_\odot$ sequence. For the 1.35 $M_\odot$ sequence, the abundance flow reaches ^{35}Ar, and ^{39}Ca, both of which are depleted by subsequent β-decays.

At this point we have performed a series of network calculations by varying independently the rates of the (p, γ) reactions on ^{27}Si, ^{31}S, ^{35}Ar, and ^{39}Ca within the uncertainties displayed in Figure 8. Our results show that rate variations for the ^{31}S + p, ^{35}Ar + p, and ^{39}Ca + p reactions have no noticeable effect on the final nova abundances for both sequences. Varying the rates for the ^{27}Si + p reaction changes the final isotopic abundances by less than 10% (5%) for the 1.25 $M_\odot$ (1.35 $M_\odot$) sequence, as can be seen in Figure 11. In order to investigate further the sensitivity of the final abundances on reaction-rate uncertainties, we performed another series of network calculations by varying reaction rates by an arbitrary factor of 10 up and down. Rate variations for the ^{31}S + p, ^{35}Ar + p, and ^{39}Ca + p reactions change the final abundances by less than 20% for both sequences. Varying the ^{27}Si + p reaction rates results in final abundance changes of less than 50%, as shown in Figure 11. We also note that none of the reaction-rate variations performed in this work have a noticeable influence on the total nuclear energy generation.

These surprising results can be understood qualitatively by discussing the (p, γ) reactions together with the competing β-decays. The solid lines in Figure 12 represent temperature and density conditions for which the (p, γ) reactions on ^{27}Si, ^{31}S, ^{35}Ar, and ^{39}Ca and the competing β-decays are of equal strengths. The solid curves are calculated by using our recommended reaction rates and by assuming a hydrogen mass fraction of $X_{\rm H} = 0.365$ (Politano et al. 1995). In the region above the solid curves the proton-capture reaction dominates, while below the solid lines the nuclei of interest here are depleted by β-decay. The dashed lines display temperature-density profiles for the two nova sequences considered, which evolve in time from large to small density values. It can be seen that ^{31}S and ^{39}Ca will be depleted by β-decays even if the proton capture reaction

TABLE 8

FINAL ABUNDANCES (MASS FRACTIONS) FOR ONeMg NOVA MODELS OBTAINED WITH RECOMMENDED REACTION RATES OF PRESENT WORK

		Model				Model	
Number	Isotope	1.25 $M_\odot$	1.35 $M_\odot$	Number	Isotope	1.25 $M_\odot$	1.35 $M_\odot$
1	^{1}H	2.4E−01	1.9E−01	18	^{26}Mg	4.9E−07	2.8E−06
2	^{4}He	2.3E−01	2.3E−01	19	^{26}Al	1.9E−03	4.6E−03
3	^{12}C	2.3E−02	6.3E−02	20	^{27}Al	1.4E−02	2.4E−02
4	^{13}C	1.9E−02	2.9E−02	21	^{28}Si	7.6E−02	1.0E−01
5	^{14}N	8.3E−02	2.4E−02	22	^{29}Si	9.8E−04	2.1E−03
6	^{15}N	2.4E−06	3.4E−03	23	^{30}Si	1.7E−02	2.6E−02
7	^{16}O	3.1E−04	1.5E−04	24	^{31}P	1.7E−02	2.2E−02
8	^{17}O	3.0E−03	2.6E−05	25	^{32}S	7.3E−02	1.5E−01
9	^{18}O	1.0E−07	1.8E−06	26	^{33}S	2.9E−04	3.1E−03
10	^{19}F	4.8E−06	1.3E−07	27	^{34}S	2.1E−04	4.1E−03
11	^{20}Ne	1.9E−01	8.9E−02	28	^{35}Cl	1.5E−04	1.0E−02
12	^{21}Ne	2.7E−06	5.5E−06	29	^{37}Cl	5.4E−06	8.4E−04
13	^{22}Ne	1.1E−06	2.4E−07	30	^{36}Ar	9.1E−06	1.9E−03
14	^{22}Na	9.9E−05	4.1E−05	31	^{37}Ar	1.7E−05	4.9E−03
15	^{23}Na	1.8E−04	5.4E−04	32	^{38}Ar	1.1E−05	2.3E−03
16	^{24}Mg	5.9E−06	3.5E−05	33	^{39}K	3.1E−06	2.3E−04
17	^{25}Mg	4.2E−03	9.8E−03	34	^{40}Ca	1.7E−05	6.2E−05

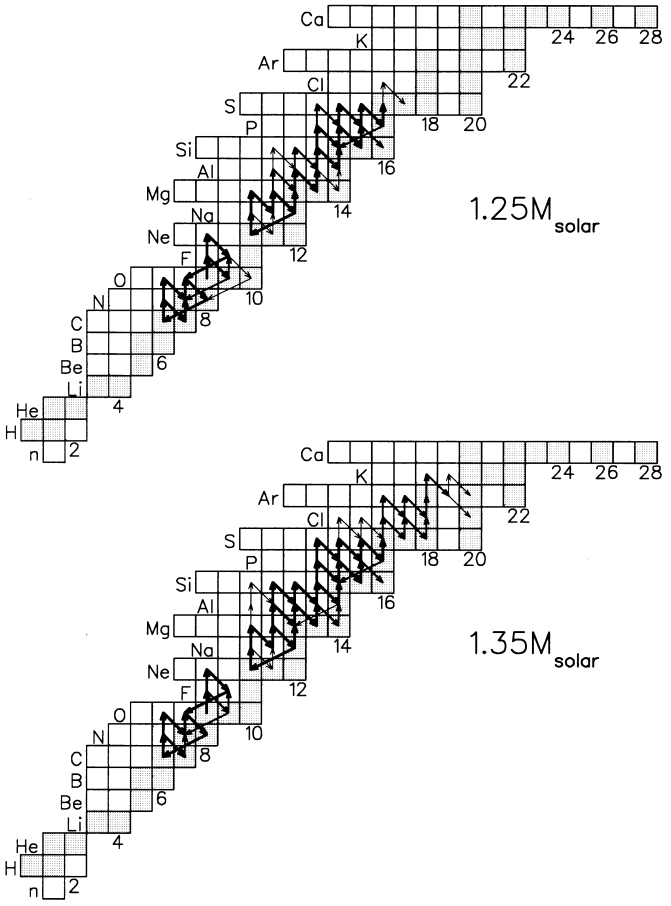

FIG. 9.—Major nuclear abundance flows F_{ij} for two nova sequences of different ONeMg white dwarf masses. The thickest solid arrows show dominant nuclear flows. Arrows of intermediate (smallest) thickness correspond to flows that are at least 1 (2) order(s) of magnitude weaker than the maximum flow. Stable isotopes are represented by shaded squares.

rates are increased by a factor of 10 (corresponding to shifting the solid curves downward by a factor of 10). Therefore, rate uncertainties for those reactions will have a negligible influence on the nucleosynthesis.

One might expect from Figure 12 that for the 1.35 $M_\odot$ sequence an increase in the $^{35}\mathrm{Ar} + p$ reaction rates by a factor of 10 will lead to a depletion of ^{35}Ar by proton capture instead of by β-decay. However, the abundance flow reaches ^{35}Ar only at times when temperature and density are already declining. Again, changing the reaction rate of $^{35}\mathrm{Ar} + p$ even by a factor of 10 will have a negligible effect on the final nova abundances. The situation is not as obvious in the case of ^{27}Si, for which the solid and dashed lines are located close to each other in Figure 12. Here, a factor of 10 increase (decrease) in the $^{27}\mathrm{Si} + p$ reaction rate will cause a depletion of ^{27}Si via proton capture reaction (β-decay) in both nova sequences. However, our network calculations indicate that the two competing sequences $^{27}\mathrm{Si}(p, \gamma)^{28}\mathrm{P}(\beta^+\nu)^{28}\mathrm{Si}$ and $^{27}\mathrm{Si}(\beta^+\nu)^{27}\mathrm{Al}(p, \gamma)^{28}\mathrm{Si}$ proceed on similar timescales, yielding relatively small changes of less than 50% in final abundances.

4.3. *Nucleosynthesis in X-Ray Bursts*

According to current theory, a type I X-ray burst is caused by the accretion of hydrogen- and helium-rich material onto the surface of a neutron star in a close binary system. Nuclear fusion reactions occur in the surface layers of the neutron star because of the high pressures exerted by the weight of the accreted matter. Since the degree of electron degeneracy in these layers is high, a thermonuclear runaway takes place and the nuclear fuel burns explosively. The nuclear energy released is transported to the surface, giving rise to the emission of X-rays for a short time. For a recent review, see Lewin et al. (1993). Although this model successfully reproduces global properties of observed bursts, such as peak luminosities and rise and recurrence timescales, certain observations remain unexplained. Among those are weak bursts with short recurrence timescales of about 5–20 minutes. Such intervals are too short for the accretion of a sufficient mass to initiate a second outburst. Therefore, it has been suggested (Lewin et al. 1993) that these weak bursts result from burning of residual hydrogen and helium that had survived previous outbursts. In general, type I X-ray bursts are not regarded as important sites of galactic nucleosynthesis, since the large gravitational potential associated with the neutron star precludes the possibility that a substantial amount of material will escape from the surface. However, it has been suggested recently (Schatz et al. 1998) that type I X-ray bursts could account for the observed solar system abundances of light p nuclei if only 0.3% of the processed matter is ejected into the interstellar medium.

In the present work, the nuclear burning is studied by using temperature and density profiles obtained from a recent hydrodynamical study (Rembges et al. 1998) of thermonuclear runaways initiated by accretion onto a neutron star with mass 1.4 $M_\odot$ and radius 10 km. Our network calculations were started at a time just prior to runaway,

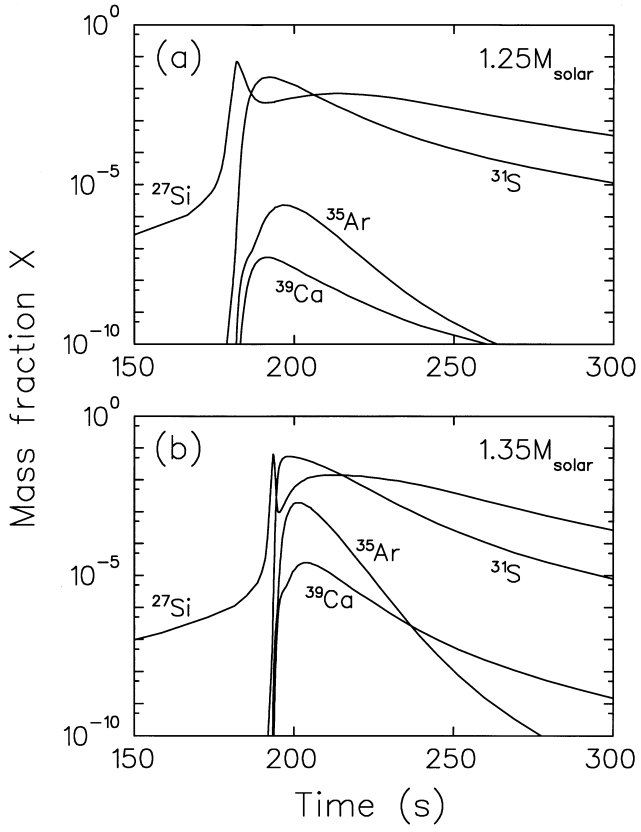

FIG. 10.—Time evolution of selected nuclear abundances during explosive nuclear burning on the surface of accreting (*a*) 1.25 $M_\odot$ and (*b*) 1.35 $M_\odot$ white dwarfs.

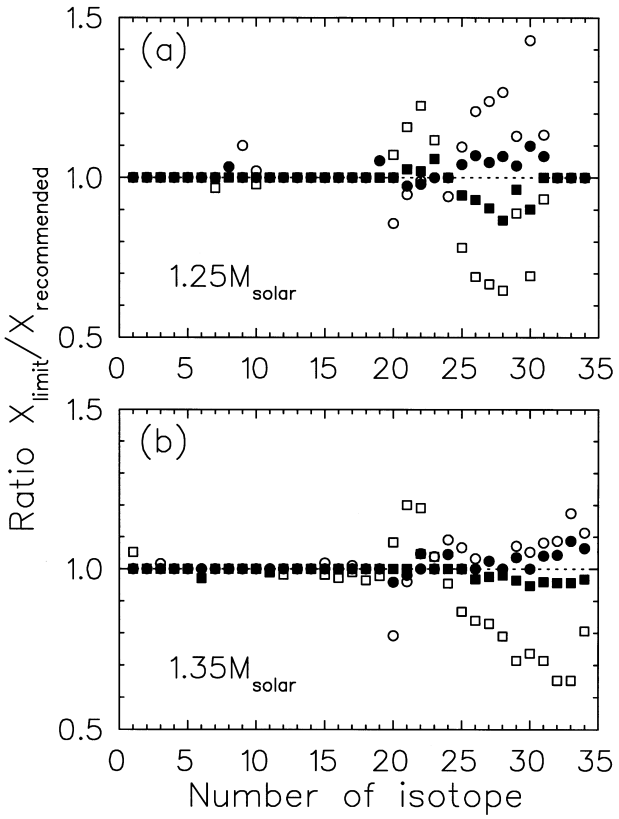

FIG. 11.—Results of $^{27}Si + p$ reaction-rate variations in explosive hydrogen burning for two different ONeMg nova sequences. Shown are ratios of final isotope abundances obtained from reaction-rate variations and our recommended rates, versus the isotope number listed in Table 8. The solid circles and squares are obtained from our 1 σ upper and lower reaction-rate limits (Fig. 8*a*), respectively. The open circles and squares result from changing the reaction rates by an arbitrary factor of 10 up and down, respectively.

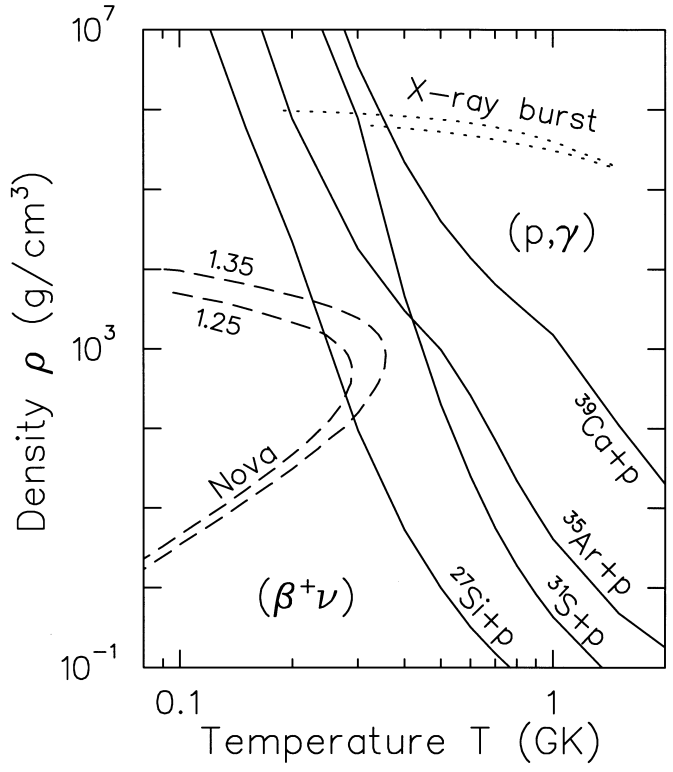

FIG. 12.—Temperature-density boundaries (*solid lines*) at which the $^{27}Si + p$, $^{31}S + p$, $^{35}Ar + p$, and $^{39}Ca + p$ reactions and the competing β-decays are of equal strength (assuming a hydrogen mass fraction of $X_H = 0.365$). The dashed lines indicate the T-ρ profiles of two nova sequences considered in this work. The nuclear-burning conditions evolve in time from larger to smaller densities. The dotted line shows the T-ρ profile of the X-ray burst model used in this work, which evolves in time from smaller to larger densities.

with temperature and density $T_9 = 0.32$ and $\rho = 6.3 \times 10^5$ g cm^{-3}, respectively, at the base of the accreted matter. The thermonuclear runaway occurs after about 1.8 s. The temperature reaches a maximum value of $T_9 = 1.5$ in the hottest burning zone after about 6 s. The nucleosynthesis is followed over a total time period of 300 s until temperatures and densities reach values of about $T_9 = 0.18$ and $\rho = 9.7 \times 10^5$ g cm^{-3}, respectively. A solar matter composition (Anders & Grevesse 1989) is assumed for the initial abundances; i.e., the accreted material consists of 98.1% (by mass) of ^{1}H and ^{4}He.

We stress again that it is not our intention to reproduce quantitatively the properties of observed type I X-ray bursts. Most burst sources are permanently active, and they show a large variety in burst profiles (Lewin et al. 1996). Therefore, more realistic studies of X-ray burst nucleosynthesis require the description of the long-term history of burst sources through many thermonuclear outbursts. For example, it has been shown previously (Taam et al. 1993, 1996; Woosley & Weaver 1985) that both the heating of surface layers and the composition of the ashes after one burst strongly influence the properties of the next thermonuclear runaway (the effects of "thermal inertia" and "compositional inertia," respectively). Furthermore, it has been argued (Wallace & Woosley 1985; Schatz et al. 1998) that nucleosynthesis and energy generation in type I X-ray bursts depend crucially on the precise knowledge of masses and β-decay half-lives for proton-rich nuclei heavier than ^{56}Ni. Unfortunately, little experimental information exists for this mass region. Therefore, stellar models have to rely on theoretical estimates. The reader is referred to Schatz et al. (1998) for a systematic study of the influence of different nuclear models on the resulting nuclear burning in type I X-ray bursts. In the present work we focus on the impact of our recommended reaction rates and their uncertainties on energy production, residual hydrogen abundance, and final isotope abundances.

Time-integrated net abundance flows F_{ij}, obtained in the present work with our recommended reaction rates (Tables 6 and 7) and temperature-density profiles of Rembges et al. (1998), are displayed in Figure 13. The flow diagram reveals the predominant nuclear processes occurring during the outburst: (1) helium is converted to carbon by the 3α process, (2) nuclei in the intermediate-mass region between oxygen and argon are processed via sequences of (α, p) and (p, γ) reactions (the so-called αp-process; Wallace & Woosley 1981), and (3) the nucleosynthesis above mass $A = 40$ is characterized by an extended network of (p, γ) reactions and β-decays. For the high temperatures and densities typical of type I X-ray bursts, proton-capture reactions on the majority of nuclei are much faster than the competing β-decays. The nuclear fuel is quickly converted by (p, γ) reactions to isotopes near the proton drip line, where further proton captures are hindered by photodisintegration. Consequently, the abundance flows have to wait for slow β-decays.

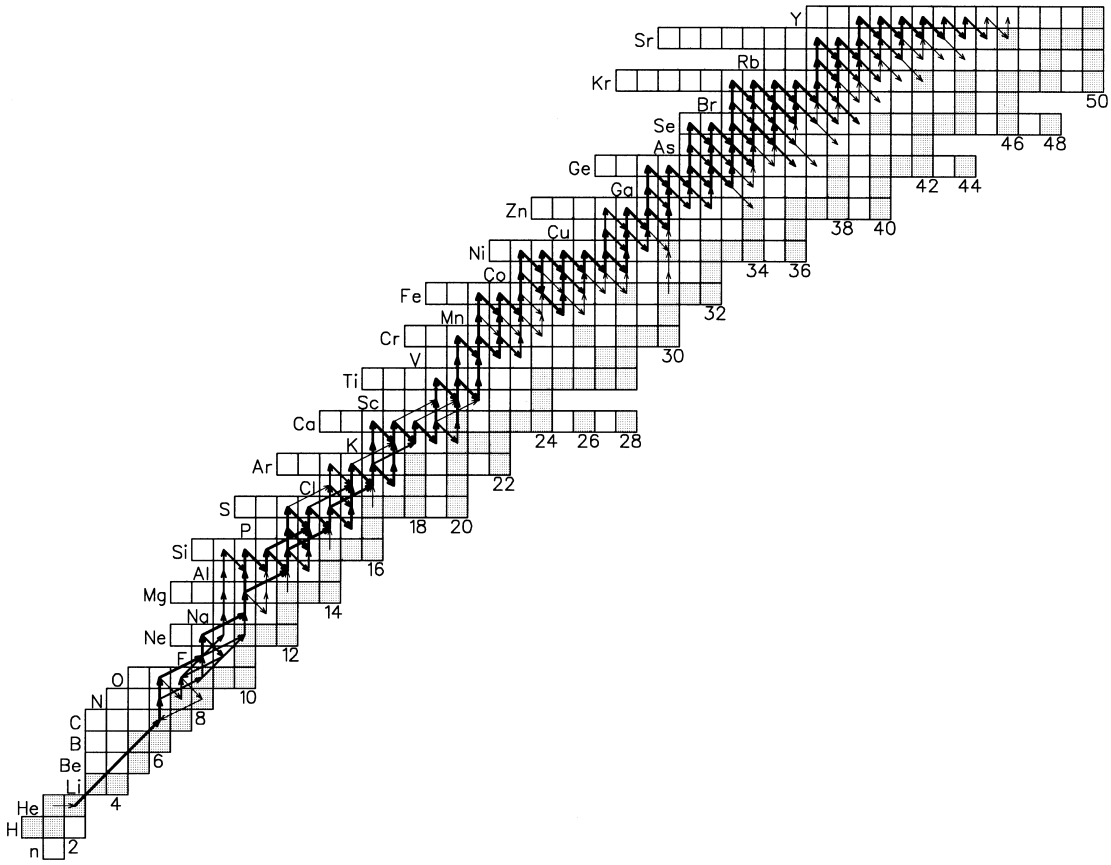

FIG. 13.—Major nuclear abundance flows F_{ij} for an X-ray burst model. The thickest solid arrows show dominant nuclear flows. Arrows of intermediate (smallest) thickness correspond to flows that are at least 1 (2) order(s) of magnitude weaker than the maximum flow. Stable isotopes are represented by shaded squares.

The operation of the αp-process in the intermediate-mass region is of great importance in this respect since (α, p) reactions can bridge certain waiting-point nuclei. Therefore, the nuclear burning of material below mass $A = 40$ proceeds at an accelerated pace and more energy can be released in the thermonuclear runaway (Wallace & Woosley 1981). The entire nuclear-burning process is influenced by those nuclei that represent the largest impedance for a continues abundance flow (Van Wormer et al. 1994). This property is apparent from the nuclear energy generation rate, displayed in Figure 14*a*. The peaks are predominantly caused by the temporary storage of material at the waiting-point nuclei ^{24}Si, ^{30}S, ^{56}Ni, ^{64}Ge, and ^{68}Se. Since the energy generation rate is proportional to the product of abundance change and nuclear energy release, energy generation maxima will occur at times when the abundances of waiting-point nuclei change most rapidly (Fig. 14*b*). Consequently, at the maxima shown in Figure 14*b* the waiting-point abundances change little and the energy generation drops, causing the peaks seen in Figure 14*a*. The waiting-point abundances are mainly depleted by β-decays (for ^{24}Si, ^{30}S, ^{64}Ge, ^{68}Se), (α, p) reactions (for ^{30}S), and proton capture reactions (for ^{56}Ni, ^{64}Ge). The total energy released by nuclear reactions and decays amounts to $\epsilon_{\rm nuc} = 4.1 \times 10^{18}$ ergs g^{-1}.

Final isotopic abundances are listed in Table 9. The residual hydrogen and helium mass fractions are 0.22 and 0.035, respectively. Isotopes in the $A = 64$–77 range account for an integrated mass fraction of $\sum X = 0.45$, with ^{68}As being the most abundant isotope at the end of our calculation. Overproduction factors for the most proton-rich stable isotope of a given mass A, defined as the ratios of our final mass fractions after all β-decays have been completed, and the corresponding solar mass fractions, $F = (X_i/X_\odot)$, are displayed in Figure 15. We note that a significant amount of material has also been transformed to nuclei in the $A = 78$–89 range, for which we list in Table 9 only the integrated mass fraction ($\sum X = 0.29$). This material would most likely be transformed to even heavier isotopes in a calculation (Schatz et al. 1998) involving a reaction network that extends beyond our end point, ^{89}Y (see § 4.1).

At this point we varied independently the rates of the (p, γ) reactions on ^{27}Si, ^{31}S, ^{35}Ar, and ^{39}Ca within the uncertainties displayed in Figure 8. Our results show that rate variations for the ^{27}Si + p, ^{31}S + p, and ^{35}Ar + p reactions have no noticeable effect on the final X-ray burst abundances. Varying the rates for the ^{39}Ca + p reaction changes final isotopic abundances by up to 55%, but only for nuclei in the mass $A = 40$–48 range. Another series of network calculations has been performed by changing the reaction rates by an arbitrary factor of 10 up and down. Rate variations for the ^{27}Si + p, ^{31}S + p, and ^{35}Ar + p reactions change final abundances by less than 40%. Varying the ^{39}Ca + p reaction rates results in final abundance changes of up to a factor of 2. Only nuclei in the mass $A = 40$–48 range are affected by these reaction-rate variations. We emphasize that none of the reaction-rate changes performed in this work have a noticeable influence on either the total energy generation or the residual hydrogen and helium abundances.

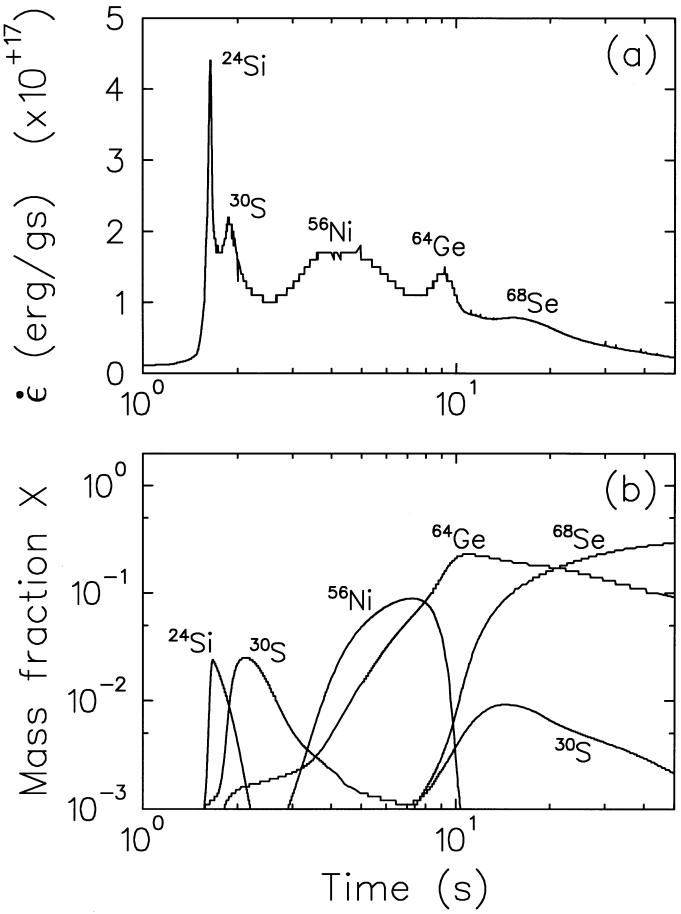

FIG. 14.—(*a*) Thermonuclear energy generation for the evolution of an accreting neutron star. (*b*) Abundance evolution of the most important waiting-point nuclei. Energy generation maxima occur approximately at time periods when the waiting-point abundances change most rapidly.

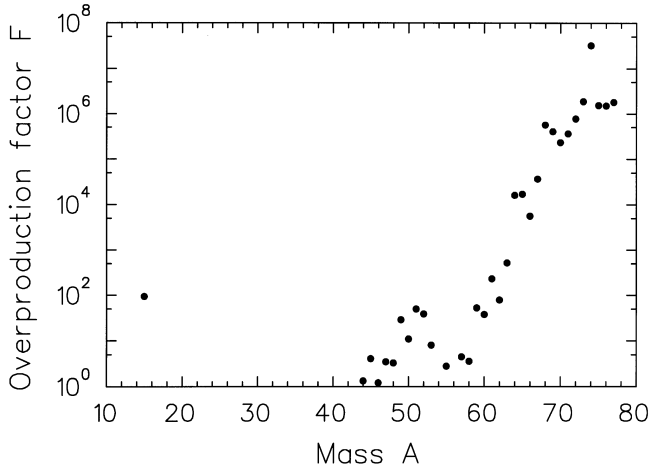

FIG. 15.—Overproduction factors F for the most proton-rich stable isotope of given mass A, obtained for an X-ray burst model by using our recommended reaction rates. The F values are defined as the ratios of final abundances after all β-decays have been completed and the corresponding solar abundances. Only values of $F \geq 1$ are displayed.

One might have expected larger effects, since part of the major abundance flow passes through the nuclei ^{27}Si, ^{31}S, ^{35}Ar, and ^{39}Ca (see Fig. 13). Our results can be understood as follows. The temperature-density profile of the X-ray burst model is shown in Figure 12 as dotted line. It is apparent that the proton capture reactions of interest here are much faster than the competing β-decays for all conditions at which significant nuclear processing occurs. In fact, the (p, γ) reactions on ^{27}S, ^{31}S, and ^{35}Ar are fast enough that material never accumulates substantially at those nuclei compared to the peak abundances of the main waiting-point nuclei (Fig. 14*b*). This is demonstrated in Figure 16, showing the time evolutions of ^{27}Si, ^{31}S, and ^{35}Ar abundances. Since the overall nucleosynthesis is mainly determined by impedances at the waiting-point nuclei, variations of the ^{27}Si + p, ^{31}S + p, and ^{35}Ar + p reaction rates will have only a small effect on the final results. When the abundance flow reaches the isotope ^{39}Ca, the material is processed in a different fashion. Since the Q value for the ^{39}Ca$(p, \gamma)^{40}$Sc reaction is small ($Q = 0.54$ MeV), the inverse photodisintegration of ^{40}Sc will compete with the proton capture reaction on ^{39}Ca. As a result, a relatively large amount of material accumulates at ^{39}Ca, as can be seen in Figure 16. The subsequent nuclear abundance flow depends mainly on the ratio of proton capture and photodisintegration reaction rates, which is determined by the reaction Q value rather than by nuclear reaction cross sections (see § 1). Consequently, variations of the ^{39}Ca + p reaction rates will have an effect on the nucleosynthesis only at time periods when the ^{39}Ca(p, γ) and ^{40}Sc(γ, p) reactions evolve into and out of equilibrium, which explains the abundance changes of $A = 40$–48 nuclei described above.

TABLE 9

FINAL ABUNDANCES (MASS FRACTIONS) FOR X-RAY BURST MODEL OBTAINED WITH RECOMMENDED REACTION RATES OF PRESENT WORK[a]

Isotope	X	Isotope	X	Isotope	X
^{1}H	2.2E−01	^{68}Ge.....	4.2E−02	^{74}Kr	2.9E−02
^{4}He	3.5E−02	^{69}As	1.5E−02	^{74}Br	4.3E−03
^{64}Ge.....	3.8E−03	^{69}Ge.....	1.2E−03	^{75}Kr	1.4E−02
^{64}Ga.....	8.6E−03	^{70}Se	1.0E−02	^{75}Br	5.4E−03
^{64}Zn	3.6E−03	^{71}Se	7.4E−03	^{76}Rb	1.1E−03
^{65}Ga.....	4.0E−03	^{71}As	2.3E−03	^{76}Kr	1.5E−02
^{66}Ge.....	3.3E−03	^{72}Br	1.6E−02	^{77}Rb	1.1E−02
^{67}Ge.....	2.8E−03	^{72}Se	3.0E−02	^{77}Kr	5.8E−03
^{68}Se	8.4E−02	^{73}Br	2.2E−02	U A = 78–89[b]	2.9E−01
^{68}As	1.0E−01	^{73}Se	1.0E−02		

[a] Listed are only isotopes with mass fractions of $X \geq 10^{-3}$.

[b] Isotopic enrichment of material due to the artificial truncation of our reaction network at the element yttrium (§ 4.1).

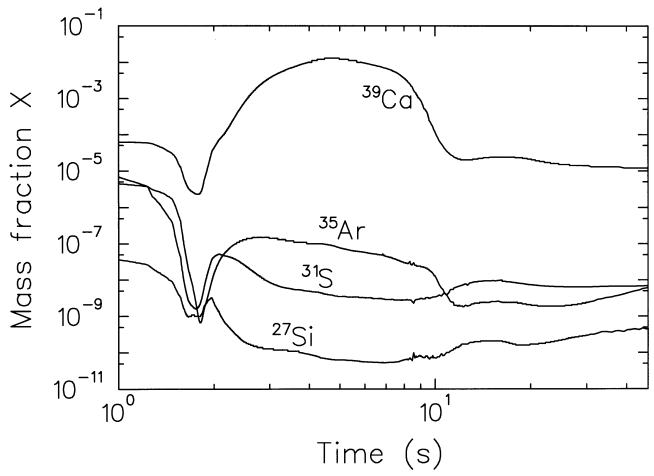

FIG. 16.—Time evolution of selected nuclear abundances during explosive nuclear burning on the surface of an accreting neutron star.

5. SUMMARY AND CONCLUSIONS

The present work describes extensive and systematic methods for estimating (p, γ) reaction rates on the radioactive target nuclei ^{27}Si, ^{31}S, ^{35}Ar, and ^{39}Ca. Our results are based on measured excitation energies of astrophysically important nuclear levels. Mirror state correspondences are obtained by using the isobaric multiplet mass equation (IMME). Application of the IMME yields reliable results for the isospin triplet states of interest in this work, mainly because experimental excitation energies of the $T_z = 0$ and 1 members of the isospin triplet are used in order to predict the E_X value of the corresponding state in the $T_z = -1$ (proton-rich) nucleus. On average, estimated and measured excitation energies in proton-rich nuclei agree to within 50 keV. Spectroscopic factors, proton partial widths and γ-ray partial widths of states belonging to the same isospin multiplet are systematically compared. It is demonstrated that the method described in Iliadis (1997) of estimating proton partial widths provides reliable results within a factor of 1.7. A procedure for assigning realistic uncertainties to reaction rates is described, and a more detailed account has been published elsewhere (Thompson & Iliadis 1999).

Our recommended reaction rates are incorporated into large-scale nuclear reaction network calculations in order to investigate the consequences for the nucleosynthesis and nuclear energy generation in novae and X-ray bursts. In addition, series of network calculations are performed by varying independently reaction rates within their assigned uncertainties. For the nuclear burning in ONeMg novae we find that reaction-rate uncertainties of proton captures on ^{27}Si, ^{31}S, ^{35}Ar, and ^{39}Ca change the calculated final abundances and the total nuclear energy generation by negligible amounts only. Even arbitrary variations in reaction rates by factors of 10, which we find unlikely in view of the present analysis, change the final abundances by less than 50%. This variation is smaller than uncertainties of observed elemental nova abundances (typically a factor of 2; S. Starrfield 1998, private communication) and cannot be regarded as substantial. For the nuclear burning in type I X-ray bursts, we have shown that uncertainties in the $^{27}\mathrm{Si} + p$, $^{31}\mathrm{S} + p$, $^{35}\mathrm{Ar} + p$, and $^{39}\mathrm{Ca} + p$ reaction rates have a negligible effect on the total nuclear energy generation and on the residual hydrogen or helium abundance. Final abundances of certain other isotopes change by less than 55%. Arbitrary reaction-rate variations by factors of 10 cause slightly larger abundance changes. However, these reaction-rate uncertainties influence only abundances of nuclei in the mass $A = 40$–48 range with very small overproduction factors (Fig. 15). Therefore, we expect only negligible astrophysical consequences, even if a fraction of the processed material escapes the large gravitational potential well of the neutron star, as speculated by Schatz et al. (1998).

In conclusion, the present study provides stellar rates for the $^{27}\mathrm{Si} + p$, $^{31}\mathrm{S} + p$, $^{35}\mathrm{Ar} + p$, and $^{39}\mathrm{Ca} + p$ reactions that are of sufficient accuracy for quantitative predictions of nuclear-burning processes in novae and X-ray bursts. Contrary to the claim of Rembges et al. (1997), we find in the present study no compelling evidence for measuring these reactions at radioactive ion beam facilities. In this work we have investigated the nucleosynthesis in the hottest hydrogen and helium-burning zone only. We cannot exclude, but it is unlikely, that a consideration of other burning zones will change our results appreciably. The reader should be aware that our results have not been obtained in a self-consistent manner. Such calculations requiring the use of a nuclear reaction network that is directly coupled to hydrodynamic evolutionary models could indeed change some of our conclusions. Finally, we note that an investigation of explosive nuclear burning in more speculative astrophysical sites not considered in the present work (e.g., supermassive star explosions or Thorne-Zytkow objects; see § 1) might provide quantitatively different results.

The authors wish to express their gratitude to F. Rembges and S. Starrfield for helpful discussions and for providing us with their temperature and density profiles. We are also grateful for the detailed review of this work by the referee, F.-K. Thielemann. This work was supported in part by the US Department of Energy under Grant DE-FG02-97ER41041.

APPENDIX A

NUCLEAR PHYSICS DATA

This appendix gives details of the nuclear physics properties used as input to the reaction-rate calculations.

A1. THE $^{27}\mathrm{Si}(p, \gamma)^{28}\mathrm{P}$ REACTION

Resonance parameters and analog assignments for this reaction are listed in Table 1. Thirteen resonances with energies $E_R \leq 1446$ keV are taken into account in calculating the reaction rates. Previously, only five resonances were considered (Wiescher et al. 1986). The γ-ray partial widths for the $E_R = 791$ and 1446 keV resonances are not known, since the lifetimes of the corresponding mirror levels in ^{28}Al were not measured. For these Γ_γ values we have adopted shell-model results (Endt &

Booten 1993). Both resonances have no significant influence on the total reaction rates. Only a lower limit could be calculated for the Γ_p value of the $E_R = 830$ keV resonance since the $\ell = 0$ component of the spectroscopic factor was not measured. This result has no influence on the resonance strength, which is dominated by the measured Γ_γ value of the mirror state. It should be noted that the neutron spectroscopic factors for the ^{28}Al levels at $E_X = 2201$ and 2272 keV that are listed in column (5) of Table 28.13 in Endt & van der Leun (1978) have to be multiplied by a factor of 6. The wrong values were used in the previous reaction-rate estimate of Wiescher at al. (1986).

A2. THE ^{31}S(p, γ)^{32}Cl REACTION

Twelve resonances with energies $E_R \leq 1822$ keV are taken into account for the calculation of reaction rates (Table 2). Only four resonances were considered previously (Vouzoukas et al. 1994). The 1_4^+ and 4_1^+ shell-model states in ^{32}Cl were not observed experimentally. Their resonance energies are calculated by using the IMME (eq. [11]), with an estimated uncertainty of about 50 keV. Both resonances have no influence on the total reaction rates. For the $E_R = 1726$ and 1822 keV resonances the neutron spectroscopic factors for the corresponding ^{32}P levels have not been measured. Upper limits for the resonance strengths are obtained with $\omega\gamma \leq \omega\Gamma_\gamma$, since $\Gamma_p/\Gamma \leq 1$. Their contributions to the total reaction rates are negligible.

A3. THE ^{35}Ar(p, γ)^{36}K REACTION

Four resonances with energies $E_R \leq 744$ keV are considered for the calculation of reaction rates (Table 3). Five additional resonances are expected below $E_R \approx 1$ MeV if the known structure of the mirror nucleus ^{36}Cl is taken into account. The resonance energies are estimated by using the IMME (eq. [11]). Resonance parameters (i.e., spectroscopic factors and lifetimes) are adopted from experimental mirror-state information. The additionally expected resonances increase the upper limits of the total reaction rates at high temperatures $T_9 \geq 1.5$ by a factor of 2 only (see § 3). Note that the $S_{\ell=0}$ neutron spectroscopic factors of ^{36}Cl levels that are listed in column (4) of Table 36.14a in Endt & van der Leun (1978) have to be multiplied by a factor of 2.

A4. THE ^{39}Ca(p, γ)^{40}Sc REACTION

Four resonances are taken into account for the calculation of the reaction rates (Table 4). Previously, only three resonances were considered (Wiescher & Görres 1989). In the ^{40}Ca(^{3}He, t)^{40}Sc study of Schulz, Alford, & Jamshidi (1971), a triplet of states was observed at $E_X = 1.67$ MeV. Only one of these states was considered in Wiescher & Görres (1989), and it was assumed that this level corresponds to the 0_1^+ state in ^{40}K. However, the IMME (eq. [11]) predicts ^{40}Sc excitation energies of $E_X = 1617$, 1683, and 1853 keV for the 1_1^-, 2_2^- and 0_1^+ states, respectively. Therefore, we identify the observed structure at $E_X = 1.67$ MeV with the 1_1^- and 2_2^- states (Table 4), which is in agreement with the work of Loiseaux et al. (1971). Four additional resonances are expected below $E_R \approx 1.3$ MeV if the level structure of the mirror nucleus ^{40}Sc is taken into account. Their contributions, which are estimated as described in the previous paragraph, increase the upper limits of the total reaction rates at high temperatures above $T_9 = 1$ by a factor of 4 (see § 3).

APPENDIX B

ON THE USE OF LOGNORMAL DISTRIBUTIONS

In the present work we estimate means and dispersions for ratios of spectroscopic factors S, proton partial widths Γ_p, and γ-ray partial widths Γ_γ (§§ 2.3 and 2.4) by using logarithmic ratios, with the relations (Möller & Randrup 1990)

$$r_l = \log_{10}(x)\,, \tag{B1}$$

$$M_r = \frac{1}{n}\sum_{i=1}^{n} r_l^i\,, \qquad M_r^{10} = 10^{M_r}\,, \tag{B2}$$

$$\sigma_r = \sqrt{\frac{1}{n}\sum_{i=1}^{n}(r_l^i - M_r)^2}\,, \qquad \sigma_r^{10} = 10^{\sigma_r}\,, \tag{B3}$$

where x stands for ratios of either S, Γ_p, or Γ_γ. The quantity M_r^{10} measures systematic trends, whereas σ_r^{10} measures the average scatter of the data around the mean value M_r^{10}. In the following we provide a statistical basis for this procedure, which, to our knowledge, has not been described previously in the nuclear astrophysics literature.

We start with the definition of the lognormal distribution for a positive variable x, $L_{\zeta,\sigma}(x)$, given by (Thompson 1997)

$$L_{\zeta,\sigma}(x) = \frac{1}{\sqrt{2\pi}\sigma x}\, e^{-(\ln x - \zeta)^2/(2\sigma^2)}\,, \tag{B4}$$

in which σ is the standard deviation of the corresponding Gaussian (normal) distribution. The quantity ζ is a fitting parameter, and the distribution is normalized to unit total probability. The x in the denominator ensures that the probability content over small intervals of x is the same in this distribution as in the normal distribution. The most probable value of the lognormal distribution occurs when $x_m = e^{\zeta-\sigma^2}$. As first pointed out by Galton (1879), the logarithm of a product of

independent positive random variables has a lognormal distribution if each variable in the product has a normal distribution. The relation of equation (B4) to estimating quantities relevant to thermonuclear reactions is as follows.

Quantities such as reaction rates and resonance widths estimated from the formulas given in § 2 can often be written as products (or quotients) of positive quantities that are obtained independently. For example, an estimated proton partial width contains the product of the following positive quantities: a penetrability, a spectroscopic factor, and a single-particle reduced width, as can be seen from equation (12). Such factors most likely have independent random errors. Assuming a normal distribution for the underlying factors, and thereby a lognormal distribution for their product, is therefore reasonable.

In the past, error estimates were often made (Endt et al. 1988; Möller & Randrup 1990) by a least-squares fitting procedure that corresponds to maximizing the likelihood function (Thompson 1992) obtained by using the modified distribution

$$L'_{\zeta,\sigma}(x) = xL_{\zeta,\sigma}(x) = \frac{1}{\sqrt{2\pi}\sigma}\, e^{-(\ln x-\zeta)^2/(2\sigma^2)}\,, \tag{B5}$$

which is a normal distribution in terms of the variable $\ln\ x$. The most probable value of this distribution occurs when

$$x'_m = e^{\zeta} = x_m\, e^{\sigma^2}\,. \tag{B6}$$

Clearly, the best-fit value of x is biased upward by the factor e^{σ^2}, which is ignored in most analyses. Apart from this error, the procedure of fitting on a logarithmic scale is appropriate. Such a bias introduced by applying logarithmic transformations to data has also been discussed elsewhere (Thompson & Macdonald 1991; Gatland & Thompson 1993).

As an example of using logarithmic distributions, consider the analysis of the ratio of experimental to calculated proton partial widths, Γ_p, presented in § 2.3 and shown in Figure 4*b*. For this data set one infers from equation (B6) a factor of $x'_m = 1.04$ for the most probable logarithmic ratio, in good agreement with the value of 1.03 calculated by using equations (B1), (B2), and (B3) and given in § 2.3. The logarithmic standard deviation is $\sigma = 0.56$, yielding a bias factor of $e^{\sigma^2} = 1.75$, again in good agreement with the factor 1.73 calculated by using equation (B3) and presented in § 2.3. Application of the true lognormal distribution, given by equation (B4), then produces $x_m = x'_m e^{-\sigma^2} = 0.76$ for the most probable value of the partial width ratio. In this example, the bias factor e^{σ^2} yields a ratio that is within the originally estimated standard deviation of 1.73.

Within the framework of Gaussian error distributions, only if data have been fitted on logarithmic scales is it appropriate to ascribe errors as factor uncertainties (multiplication or division) rather than additive or subtractive uncertainties. Even then, the bias factor e^{σ^2} in equation (B6) should always be considered if the common distribution $L'_{\zeta,\sigma}(x)$ in equation (B5) is used instead of the more appropriate lognormal distribution $L_{\zeta,\sigma}(x)$, given by equation (B4).

REFERENCES

Anders, E., & Grevesse, N. 1989, Geochim. Cosmochim. Acta, 53, 197
Arai, K., & Hashimoto, M. 1995, A&A, 302, 99
Arnett, W. D., & Truran, J. W. 1969, ApJ, 157, 339
Audi, G., & Wapstra, A. H. 1995, Nucl. Phys. A, 595, 409
Benenson, W., & Kashy, E. 1979, Rev. Mod. Phys., 51, 527
Biehle, G. T. 1991, ApJ, 380, 167
Brown, B. A., Etchegoyen, A., & Rae, W. D. M. 1985, MSU/NSCL-Report 524
Brussaard, P. J., & Glaudemans, P. W. M. 1977, Shell-Model Applications in Nuclear Spectroscopy (Amsterdam: North-Holland)
Cannon, R. C. 1993, MNRAS, 263, 817
Champagne, A. E., Brown, B. A., & Sherr, R. 1993, Nucl. Phys. A, 556, 123
Champagne, A. E., & Wiescher, M. 1992, Annu. Rev. Nucl. Part. Sci., 42, 39
Coszach, R., et al. 1995, Phys. Lett. B, 353, 184
Decrock, P., et al. 1993, Phys. Rev. C, 48, 2057
Delbar, T., et al. 1993, Phys. Rev. C, 48, 3088
Endt, P. M. 1990, Nucl. Phys. A, 521, 1
———. 1998, Nucl. Phys. A, 633, 1
Endt, P. M., & Booten, J. G. L. 1993, Nucl. Phys. A, 555, 499
Endt, P. M., De Wit, P., Alderliesten, C., & Wildenthal, B. H. 1988, Nucl. Phys. A, 487, 221
Endt, P. M., & van der Leun, C. 1978, Nucl. Phys. A, 310, 1
Fang, D. F. 1987, Ph.D. thesis, Fudan Univ.
Fang, D. F., Bilpuch, E. G., Westerfeld, C. R., & Mitchell, G. E. 1988, Phys. Rev. C, 37, 28
Fowler, W. A., Caughlan, G. R., & Zimmerman, B. A. 1967, ARA&A, 5, 525
Fuller, G. M., Woosley, S. E., & Weaver, T. A. 1986, ApJ, 307, 675
Galton, F. 1879, Proc. R. Soc. London, 29, 365
Gatland, I. R., & Thompson, W. J. 1993, Am. J. Phys., 61, 269
Gehrz, R. D., Truran, J. W., Williams, R. E., & Starrfield, S. 1998, PASP, 110, 3
Glendenning, N. K. 1983, Direct Nuclear Reactions (New York: Academic)
Graff, S., Görres, J., Wiescher, M., Azuma, R. E., King, J., Vise, J., Hardie, G., & Wang, T. R. 1990, Nucl. Phys. A, 510, 346
Herndl, H., Fantini, M., Iliadis, C., Endt, P. M., & Oberhummer, H. 1998, Phys. Rev. C, 58, 1798
Herndl, H., Görres, J., Wiescher, M., Brown, B. A., & Van Wormer, L. 1995, Phys. Rev. C, 52, 1078
Iliadis, C. 1997, Nucl. Phys. A, 618, 166
Iliadis, C., Buchmann, L., Endt, P. M., Herndl, H., & Wiescher, M. 1996, Phys. Rev. C, 53, 475
Iliadis, C., Giesen, U., Görres, J., Wiescher, M., Graff, S. M., Azuma, R. E., & Barnes, C. A. 1992a, Nucl. Phys. A, 539, 97
Iliadis, C., Ross, J. G., Görres, J., Wiescher, M., Graff, S. M., & Azuma, R. E. 1992b, Phys. Rev. C, 45, 2989
Iliadis, C., et al. 1993, Nucl. Phys. A, 559, 83
———. 1994, Nucl. Phys. A, 571, 132
Jänecke, J. 1969, in Isospin in Nuclear Physics, ed. D. H. Wilkinson (Amsterdam: North-Holland)
Jin, L., Arnett, W. D., & Chakrabarti, S. K. 1989, ApJ, 336, 572
Lewin, W. H. G., van Paradijs, J., & Taam, R. E. 1993, Space Sci. Rev., 62, 223
Loiseaux, J. M., Bruge, G., Kossanyi-Demay, P., Ha, D. L., Chaumeaux, A., Terrien, Y., & Schaeffer, R. 1971, Phys. Rev. C, 4, 1219
Möller, P., & Randrup, J. 1990, Nucl. Phys. A, 514, 1
Nelson, R. O., Bilpuch, E. G., Westerfeld, C. R., & Mitchell, G. E. 1984a, Phys. Rev. C, 29, 1656
———. 1984b, Phys. Rev. C, 30, 755
Ormand, W. E., & Brown, B. A. 1989, Nucl. Phys. A, 491, 1
Politano, M., Starrfield, S., Truran, J. W., Weiss, A., & Sparks, W. M. 1995, AJ, 448, 807
Prantzos, N., Arnould, M., & Arcoragi, J.-P. 1987, ApJ, 315, 209
Rauscher, T., Thielemann, F.-K., & Kratz, K.-L. 1997, Phys. Rev. C, 56, 1613
Rehm, K. E., et al. 1996, Phys. Rev. C, 53, 1950
———. 1998, Phys. Rev. Lett., 80, 676
Rembges, F., Freiburghaus, C., Rauscher, T., Thielemann, F.-K., Schatz, H., & Wiescher, M. 1997, ApJ, 484, 412
Rembges, J.-F., Liebendörfer, M., Thielemann, F.-K., Schatz, H., & Wiescher, M. 1998, in Stellar Evolution, Stellar Explosions and Galactic Chemical Evolution, ed. A. Mezzacappa (New York: IOP), 495
Rolfs, C. 1973, Nucl. Phys. A, 217, 29
Ross, J. G., et al. 1995, Phys. Rev. C, 52, 1681
Schatz, H., et al. 1998, Phys. Rep., 294, 167
Schulz, N., Alford, W. P., & Jamshidi, A. 1971, Nucl. Phys. A, 162, 349

Starrfield, S., Truran, J. W., Politano, M., Sparks, W. M., Nofar, I., & Shaviv, G. 1993, Phys. Rep., 227, 223
Starrfield, S., Truran, J. W., Wiescher, M. C., & Sparks, W. M. 1998, MNRAS, 296, 502
Stegmüller, F., Rolfs, C., Schmidt, S., Schulte, W. H., Trautvetter, H. P., & Kavanagh, R. W. 1996, Nucl. Phys. A, 601, 168
Taam, R. E., Woosley, S. E., & Lamb, D. Q. 1996, ApJ, 459, 271
Taam, R. E., Woosley, S. E., Weaver, T. A., & Lamb, D. Q. 1993, ApJ, 413, 324
Thompson, W. J. 1992, Computing for Scientists and Engineers (New York: Wiley)
———. 1997, Atlas for Computing Mathematical Functions (New York: Wiley)
Thompson, W. J., & Iliadis, C. 1999, Nucl. Phys. A, 647, 259
Thompson, W. J., & Macdonald, J. R. 1991, Am. J. Phys., 59, 854
Vanhoy, J. R., Bilpuch, E. G., Westerfeld, C. R., & Mitchell, G. E. 1987, Phys. Rev. C, 36, 920
Van Wormer, L., Görres, J., Iliadis, C., & Wiescher, M. 1994, ApJ, 432, 326
Vogelaar, R. B. 1989, Ph.D. thesis, Caltech
Vouzoukas, S., et al. 1994, Phys. Rev. C, 50, 1185
Wagoner, R. V. 1969, ApJ, 162, 247
Wallace, R. K., & Woosley, S. E. 1981, ApJS, 45, 389
———. 1985, in AIP Conf. Proc. 115, High-Energy Transients in Astrophysics, ed. S. E. Woosley (New York: AIP), 319
Warburton, E. K., & Weneser, J. 1969, Isospin in Nuclear Physics, ed. D. H. Wilkinson (Amsterdam: North-Holland)
Weiss, A., & Truran, J. W. 1990, A&A, 238, 178
Wiescher, M., & Görres, J. 1989, ApJ, 346, 1041
Wiescher, M., Görres, J., Thielemann, F.-K., & Ritter, H. 1986, A&A, 160, 56
Woosley, S. E., & Weaver, T. A. 1985, in AIP Conf. Proc. 115, High-Energy Transients in Astrophysics, ed. S. E. Woosley (New York: AIP), 273
Zhou, X. G., Dejbakhsh, H., Gagliardi, C. A., Jiang, J., Trache, L., & Tribble, R. E. 1996, Phys. Rev. C, 53, 982